REPORT DOCUMENTATION PAGE

AFRL-SR-BL-TR-99-

0292

1. AGENCY USE ONLY (Leave blank)	2. REPORT DATE	3. REPORT TYPE
	October 28, 1999	Final

4. TITLE AND SUBTITLE

LAMINATED MATRIX COMPOSITES - A NEW CLASS OF MATERIALS

5. FUNDING NUMBERS

Grant Number:
F49620-96-1-0321

6. AUTHOR(S)

W. Jack Lackey, Elliot Pickering, Harry King,
Stephen Crain, Mark Renier, and Lisa Ditter-Hoskins

7. PERFORMING ORGANIZATION NAME(S) AND ADDRESS(ES)

George W. Woodruff School of Mechanical Engineering
Georgia Institute of Technology
Atlanta, Georgia 30332-0405

8. PERFORMING ORGANIZATION REPORT NUMBER

E25-A18-4

9. SPONSORING / MONITORING AGENCY NAME(S) AND ADDRESS(ES)

Dr. Alexander Pechenik
AFOSR / NA
801 North Randolph Street, Room 732
Arlington, Virginia 22203

10. SPONSORING / MONITORING AGENCY REPORT NUMBER

11. SUPPLEMENTARY NOTES

12a. DISTRIBUTION / AVAILABILITY STATEMENT

Unlimited

12b. DISTRIBUTION CODE

13. ABSTRACT *(Maximum 200 Words)*

A new type of composite, which consists of a reinforcement phase plus a matrix composed of many alternate thin layers of two different materials, has been prepared. CVI appears to be an appropriate process for the fabrication of this class of materials. We have successfully fabricated such a composite using the forced flow-thermal gradient CVI process. A carbon 2-D cloth preform was infiltrated with alternate layers of C and SiC having thicknesses of 0.01 to 0.5 μm. Composites containing inexpensive SiC particles or platelets rather than fibrous reinforcement were also prepared. For a fixed cycle time, layer thicknesses increased with distance from the fiber surface. Crack deflection patterns indicate that the laminated matrix may contribute to mechanical toughness. The latter half of the project emphasized the CVD of Ti_3SiC_2 which may be a useful fiber-matrix interface coating and/or matrix material. Ti_3SiC_2 was successfully deposited onto graphite substrates, and more recently on C and SiC cloth substrates. The reagent system $TiCl_4$-$SiCl_4$-CCl_4-H_2 was used.

14. SUBJECT TERMS

Ceramics, composites, fiber-reinforced, processing, laminated

15. NUMBER OF PAGES

16. PRICE CODE

17. SECURITY CLASSIFICATION OF REPORT	18. SECURITY CLASSIFICATION OF THIS PAGE	19. SECURITY CLASSIFICATION OF ABSTRACT	20. LIMITATION OF ABSTRACT
Unclassified	Unclassified	Unclassified	UL

LAMINATED MATRIX COMPOSITES - A NEW CLASS OF MATERIALS

GRANT NUMBER F49620-96-1-0321

W. Jack Lackey, Elliot Pickering, Harry King,
Stephen Crain, Mark Renier, and Lisa Ditter-Hoskins

George W. Woodruff School of Mechanical Engineering
Georgia Institute of Technology
Atlanta, Georgia 30332-0405

Introduction

It is well-known that ceramics have desirable properties- such as lightweight, high stiffness, corrosion/wear resistance, and strength retention at high temperatures. However, their brittleness limits their use in most structural applications. Metals have excellent toughness but typically suffer from loss of strength at high temperatures, excessive creep, and high density. These shortcomings have been partially overcome for ceramics and metals using fibers or whiskers as reinforcement and also in metals using platelets and particulates. For example, the toughness of SiC and carbon have been improved by reinforcement with SiC and carbon fibers. Also, SiC fibers or platelets have been used to reinforce Ti, Al, and other metals. In these prior examples, the matrix was either single phase or contained a dispersed phase.

It is also well-known that the mechanical properties of structures can be enhanced by using alternate layers of two materials. Examples of such laminated materials include Ni/Cu, Fe/Cu, ZrO_2/Al_2O_3, SiC/C, TiC/TiN, TiC/TiB_2, TiC/Ni, Al_2O_3/Nb, and many others. Many of these systems, particularly those with very thin layers, reveal the superlattice structure. For most structures, it is clear that the mechanical and tribological properties improve significantly as layer thicknesses decrease, often rapidly as the layer thickness approaches ~0.02 μm.

The present work was undertaken to combine the advantages of fiber or particulate reinforcement and laminated structures. The resulting composite would have a reinforcement phase and a laminated matrix. It is suggested that this new class of composites be termed "Laminated Matrix Composites" (LMC). We have shown that laminated matrix composites containing C fibers in a C+SiC matrix can be fabricated by the chemical vapor infiltration (CVI) process.[1] Such a material should have improved resistance to oxidation compared to carbon-carbon. A more oxidation-resistant material might utilize SiC fibers. Even further improvement in oxidation resistance might result from the replacement of the carbon matrix layers with Ti_3SiC_2. This ternary ceramic compound has a layered crystal structure and mechanical properties similar to graphite, but superior oxidation resistance.[2-5] It has been fabricated by solid state synthesis and by CVD.[6-13]

We used computerized thermodynamic calculations to permit the construction of ternary deposition diagrams for the CVD of Ti_3SiC_2. That research has been published[14]. Using that information plus prior knowledge[3,6,7,13,15] of the CVD of Ti_3SiC_2, we completed an experimental study of the CVD of Ti_3SiC_2.

Over 40 preliminary CVD experiments were performed in an effort to verify the results of previous authors. Conditions for these preliminary experiments covered a wide composition range from 5-30% CCl_4, 25-55% $TiCl_4$, and 25-60 % $SiCl_4$, temperatures from 1000-1400°C, and hydrogen dilutions between 10-40. Several months of experimentation resulted in deposits containing only TiC or SiC. Only after increasing hydrogen dilution above 25 was Ti_3SiC_2 finally deposited. Based on these initial results, the following statistically designed experimental study of the CVD of Ti_3SiC_2 was planned.

Experimental Procedure

Four reagent compositions for the present study were chosen where previous CVD of Ti_3SiC_2 was achieved. The flow rate of hydrogen was kept constant at 2000 sccm. This was done in order to limit variations in substrate temperature from experiment to experiment due the cooling effect of flowing gas, and to minimize variation in the static gas boundary layer adjacent to the substrate. Because the total hydrogen flow remained fixed while the total reagent flow varied, hydrogen dilution, α, varied from 42.1 to 32.0. The four reagent compositions were repeated at three different temperatures (1373, 1473, 1573K) for a total of twelve experiments. Pressure and run time were kept constant at 300 torr and 150 minutes, respectfully. Table 1 shows run conditions listing flow rates, pressure, run time, α, and temperature for each experiment.

The deposition apparatus was a vertical, hot-walled reactor resistively heated with a graphite heating element. The substrates were ATJ graphite cut to 20.5 x 5.1 x 58.5 mm, and suspended ~90 mm above the gas injector. The tetrachloride reagents are liquids at room temperature and were vaporized using hydrogen as the carrier gas. Each vaporizer was equipped with a thermocouple and pressure gauge. Hydrogen flow to the vaporizers was adjusted according to the partial pressures of the reagents and controlled with MKS mass flow controllers. Excess hydrogen was routed through a separate line. Actual reagent flow rates were determined by weight loss of the vaporizer from beginning to end of an experiment.

Results

Table 2 gives the results from the study, listing run numbers with actual flow rates, deposition temperature, deposited phases as determined by XRD and EDS, and coating thickness. Ti_3SiC_2 was never found as a single phase, even though XRD patterns for experiments at 1300°C suggest otherwise. SEM showed the microstructure of these films was quite complicated, involving co-deposition of Ti_3SiC_2 with TiC and small amounts of $TiSi_2$ in some cases. Ti_3SiC_2 deposits were highly textured, with the basal planes preferentially oriented perpendicular to the substrate. Calculated flow rates show this study covered reagent compositions from 19-28% CCl_4, 30-45% $TiCl_4$ and 32-46% $SiCl_4$, and hydrogen dilution from 31-44. Ti_3SiC_2 was successfully deposited over most of this composition range. At 1300°C films showed large grained, highly textured Ti_3SiC_2, while at 1100°C Ti_3SiC_2 was co-deposited with TiC. Continuous planes of $TiSi_2$ parallel to the substrate surface appear at 1200 and 1100°C, but were believed to be caused by fluctuations in reagent composition through the course of the experiment. Coating thickness varied from 99-215 μm. The character of the deposited films and the morphology of the Ti_3SiC_2 in the films was highly temperature-dependent.

Table 1. Run Conditions for CVD of Ti_3SiC_2

Run Number	Target Flow Rates (sccm) $TiCl_4$	$SiCl_4$	CCl_4	H_2	α	Temperature (°C)	Pressure (torr)	Time (min)
1,9,5	17.5	17.5	12.5	2000	42.1	1100,1200,1300	300	150
2,10,6	25.0	17.5	12.5	2000	36.4	1100,1200,1300	300	150
3,11,7	17.5	25.0	12.5	2000	36.4	1100,1200,1300	300	150
4,12,8	25.0	25.0	12.5	2000	32.0	1100,1200,1300	300	150

Table 2. Results from Ti_3SiC_2 CVD Study

Run No.	Run Designation	Actual Flow Rates (sccm) $TiCl_4$	$SiCl_4$	CCl_4	H_2	α	Temp (°C)	Phases Identified With XRD and EDS	Coating Thickness (μm)
1	EP29	16.46	16.27	10.88	2000	41.9	1100	Ti_3SiC_2, TiC	184
2	EP23	21.10	16.60	10.00	2000	41.9	1100	Ti_3SiC_2, TiC	99
3	EP26	17.50	24.30	14.20	2000	35.7	1100	Ti_3SiC_2, TiC, $TiSi_2$	160
4	EP32	23.32	23.31	10.78	2000	34.8	1100	Ti_3SiC_2, TiC	161
5	EP24	16.70	17.80	11.08	2000	43.8	1300	Ti_3SiC_2, TiC	143
6	EP31	24.73	19.26	15.06	2000	33.9	1300	Ti_3SiC_2, TiC, $TiSi_2$	209
7	EP27	17.50	24.40	11.30	2000	37.4	1300	Ti_3SiC_2, TiC	197
8	EP22	22.92	22.25	12.73	2000	34.5	1300	Ti_3SiC_2, TiC	175
9	EP25	17.50	17.70	13.40	2000	41.1	1200	Ti_3SiC_2, TiC	129
10	EP19	24.10	18.73	11.76	2000	36.6	1200	Ti_3SiC_2, TiC, $TiSi_2$	215
11	EP15	16.70	26.03	13.89	2000	35.3	1200	Ti_3SiC_2, TiC	144
12	EP14	24.26	24.98	14.09	2000	31.6	1200	Ti_3SiC_2, TiC	171

X-Ray Diffraction

Figure 1 shows an XRD pattern for run EP31 which was deposited at 1300°C. Only Ti_3SiC_2 peaks are evident. It is representative of two other high temperature experiments, EP24 and EP27. All show a great deal of preferred crystallographic orientation.

Microstructure

Various microstructural characteristics are evident at different temperatures. Figure 2 shows a) the surface morphology, and b) the fractured cross section of Ti_3SiC_2 grown at 1300°C. The coating is highly oriented and characterized by large, plate-like grains oriented perpendicular to the substrate. This corroborates the preferred orientation seen with x-ray diffraction.

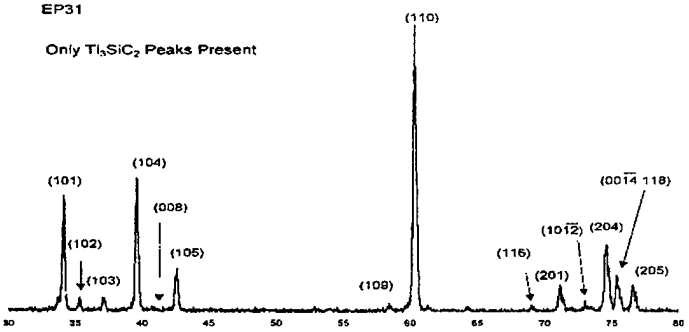

Figure 1. XRD pattern for EP31 deposited at 1300°C. Only Ti_3SiC_2 peaks are evident and peaks from basal planes show little intensity. This suggests highly textured Ti_3SiC_2.

Regions of the coating appear to have the flat side of the plate parallel to the fracture surface, while other regions appear to show the plate edge on. The surface morphology is similar in appearance to the Ti_3SiC_2 coating structure reported by Goto and Hirai.[7] The surface is an intricate pattern of grains, which are oriented in random directions. Taken together, these micrographs suggest that although the basal planes are oriented perpendicular to the substrate, there does not appear to be additional restrictions on the growth of Ti_3SiC_2. Figure 3 shows the a) surface morphology and b) fractured cross section of a coating grown at 1100°C. XRD suggests the sample is a mixture of Ti_3SiC_2 and TiC but individual phases and grains are not discernable at this magnification. Instead the coating cross section appears rather featureless. The surface appears to consist of small, nodule-like features growing on larger nodules. Compared with Figure 2, the microstructure is much finer. There is clearly a marked difference in deposition of highly oriented, large grained Ti_3SiC_2 at 1300°C and the fine grained co-deposition of TiC and Ti_3SiC_2 at 1100°C.

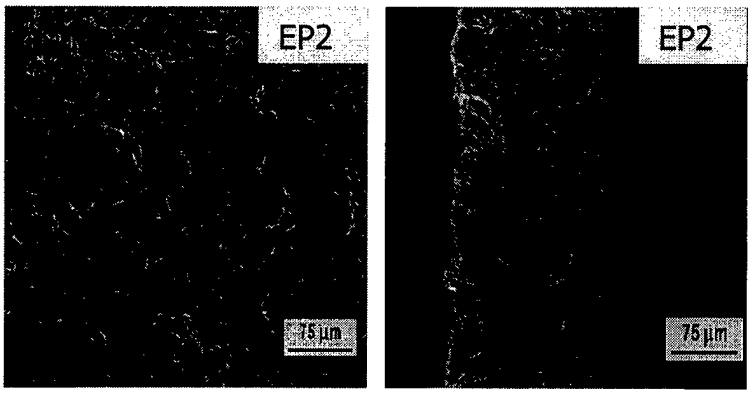

Figure 2. a) Surface morphology and b) cross section of coatings grown at 1300°C.

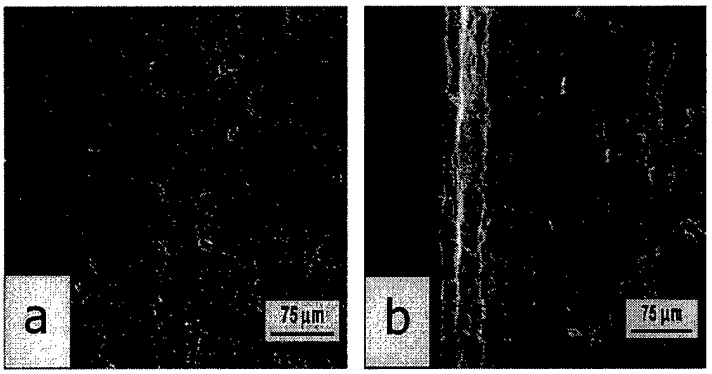

Figure 3. a) Surface morphology and
b) cross section of coatings grown at 1100°C.

Polished and etched cross sections revealed more details about the microstructure of these coatings. Figure 4 is a series of micrographs taken from experiments performed at 1100°C. Figure 4a shows the cross section of an over etched sample. The vertical bands running parallel to the substrate are the result of different etch rates on the different phases. EDS has shown these bands to be composed of Ti_3SiC_2, TiC and $TiSi_2$, again confirming data from XRD. Figure 4b was taken at higher magnification. Continuous layers of $TiSi_2$ appear early in the growth process, and are believed to be caused by fluctuations in reagent flow rates. As the carbon content of the reagent mix becomes too low, $TiSi_2$ begins to form at the leading edge of the growing surface. The remainder of the coating consists of Ti_3SiC_2 and TiC growing simultaneously, as shown in Figure 4c. The layered crystal structure is apparent in the Ti_3SiC_2 grains, identified with EDS.

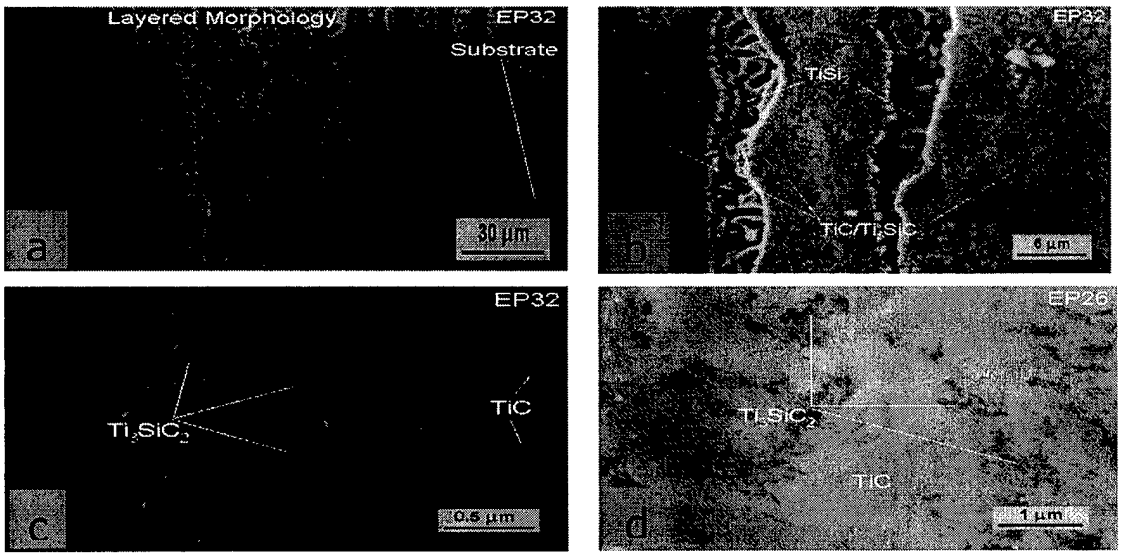

Figure 4. SEM micrographs of polished and etched cross sections of films grown at 1100°C showing a) layers of TiC, Ti_3SiC_2, and $TiSi_2$ formed by differing etch rates, b) continuous $TiSi_2$ layers and TiC/Ti_3SiC_2 co-deposition, c) high resolution of Ti_3SiC_2 grains in TiC matrix, and d) lower resolution Ti_3SiC_2 grains in TiC matrix.

Surrounding these grains are regions of TiC. The EDS spectrum from the TiC shows some silicon, but not enough to suggest Ti_3SiC_2. It is not clear whether the silicon signal is due to solid solubility of silicon in TiC or due to Ti_3SiC_2 grains hidden beneath the polished surface. Finally, Figure 4d also shows the microstructure of this two phase

region at a lower magnification. The dark phase was identified with EDS as Ti_3SiC_2, while the lighter, matrix phase was identified as TiC.

Figure 5 shows a series of micrographs for 1300°C experiments. Figure 5a is the polished and etched cross section of one of these coatings. The layered structure growing perpendicular to the substrate in fan-like grains is readily apparent. A boundary layer appears between these grains and the substrate. EDS identified this boundary layer as TiC with a small amount of silicon. A similar layer appears midway through the coating, parallel to the substrate, but much thinner. It is labeled the "intermittent layer". EDS shows this to be TiC as well. Figure 5b shows the interface between this TiC layer and Ti_3SiC_2 grains at high magnification. Notice how individual layers of the Ti_3SiC_2 grow directly into the TiC layer. The absence of a clear grain boundary between the TiC layer and Ti_3SiC_2 suggests a semi-coherent interface. Figure 5d shows the fan-like structure of Ti_3SiC_2 grains. Notice the cracks initiating in the "hilt" of the fan, and extending outward in a straight line, guided by individual layers of the grain. This demonstrates the crack deflecting properties of layered Ti_3SiC_2. These grains appear to consist of a light and a dark phase, even though the layered appearance of the structure suggests Ti_3SiC_2, alone. EDS on individual layers showed the lighter phase too silicon deficient to be Ti_3SiC_2. Instead, the grain may consist of sandwiched layers of TiC and Ti_3SiC_2.

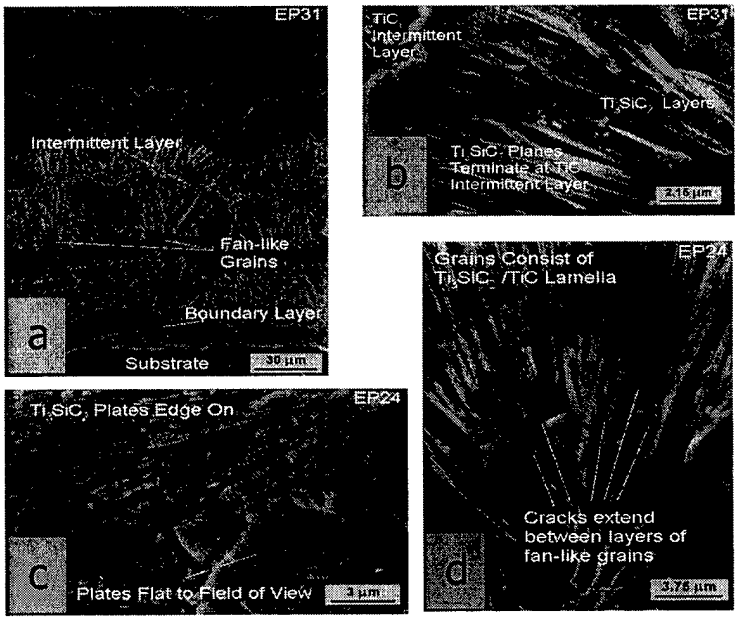

Figure 5. SEM micrographs of polished and etched cross sections of films grown at 1300°C showing a) TiC boundary and intermittent layers between fan-like grains of Ti_3SiC_2, b) interface between Ti_3SiC_2 and intermittent TiC layer, c) Ti_3SiC_2 grains seen with various orientation, and d) crack deflection in Ti_3SiC_2 and lamella structure of fan-like grains.

Summary and Conclusions

The CVD experimental study provided interesting results. Ti_3SiC_2 was successfully deposited for only the fourth time in over twenty-five years. Nearly pure Ti_3SiC_2 was deposited at 1300°C while Ti_3SiC_2-TiC composites were co-deposited at 1100 and 1200°C. At high temperature, a TiC boundary layer formed between the coating and the substrate, and periodically a thinner TiC layer was formed between regions of Ti_3SiC_2. Also, at least some of the Ti_3SiC_2 grains formed as a lamella structure with

TiC. This would suggest that the nucleation and growth of Ti_3SiC_2 is somewhat dependent on TiC. At all temperatures, Ti_3SiC_2 showed considerable preferred orientation, in which basal planes were deposited perpendicular to the substrate. Significant effort was focused on determining the temperature dependence of this orientation. Our results showed that at least some Ti_3SiC_2 was deposited with basal planes parallel to the substrate at 1100-1200°C. Additional details of this research are available.[16]

Using the results as guidelines, we have recently succeeded in the deposition of Ti_3SiC_2 onto T-300 carbon cloth and Nicalon SiC cloth. The coating was highly crystalline in each case. Some deposition conditions appear to produce a coating that readily debonds from the fiber.

Acknowledgement / Disclaimer

This work was sponsored in part by the Air Force Office of Scientific Research, USAF, under Grant No. F49620-96-1-0321. The views and conclusions contained herein are those of the authors and should not be interpreted necessarily as representing the official policies or endorsements, either expressed or implied, of the Air Force Office of Scientific Research or the United States government.

References

1. W. J. Lackey, S. Vaidyaraman, and K. L. More, "Laminated C-SiC Matrix Composites Produced by CVI," Journal of American Ceramic Society, 80[1], 113-116 (1997).
2. M. W. Barsoum, T. El-Raghy, "Synthesis and Characterization of a Remarkable Ceramic: Ti_3SiC_2" Journal of American Ceramic Society, 79[7], 1953-1956 (1996).
3. T. El-Raghy, A. Zavaliangos, M. W. Barsoum, and S. R. Kalidindi, "Damage Mechanisms Around Hardness Indentations in Ti_3SiC_2," Journal of American Ceramic Society, 80[2], 513-516 (1997).
4. M. W. Barsoum, T. El-Raghy, and D. Brodkin, "Layered Machinable Ceramics for High Temperature Applications," submitted to Scripta Materials.
5. M. W. Barsoum, T. El-Raghy, "Oxidation of Ti_3SiC_2 in Air," submitted to J. Electrochemical Soc.
6. C. Racault, F. Langlais, R. Naslain, and Y. Kihn, "On the Chemical Vapor Deposition of Ti_3SiC_2 from $TiCl_4SiCl_4CH_4H_2$ Gas Mixture: Part II, An Experimental Approach," Journal of Materials Science, 29[15], 3941-3948 (1994).
7. T. Goto, T. Hirari, "Chemical Vapor Deposition of Ti_3SiC_2," Mat. Res. Bull., 22, 1195-1201 (1987).
8. W. Jeitschoko, H. Nowotny, "Die Kristallstructur von Ti_3SiC_2-Ein Neuer Komplexcarbid-Typ," Monatash. Chem., 98, 329-337 (1967).
9. S. Arunajetesan, A. H. Carim, "Synthesis of Titanium Silicon Carbide," Journal of American Ceramic Society, 78[3], 667-672 (1995).
10. X. Tong, T. Okano, T. Iseki, and T. Yano, "Synthesis and High Temperature Mechanical Properties of Ti_3SiC_2/SiC Composite," Journal of Materials Science, [30], 3087-3090 (1995).

11. C. Racault, F. Langlais, and R. Naslain, "Solid State Synthesis and Characterization of the Ternary Phase Ti_3SiC_2," Journal of Materials Science, 29[13], 3384-3391 (1994).
12. R. Radhakrishnan, C. H. Henager, J. L. Brimhall, and S. B. Bhaduri, "Synthesis of Ti_3SiC_2/SiC and $TiSi_2$/SiC Composites Using Displacement Reactions in the Ti-Si-C System," Scripta Materialia, 34[12], 1809-1814 (1996).
13. J. Nickl, K. K. Schweitzer, and P. Luxenberg, "Chemical Vapor Deposition of the System Ti-Si-C and Ti-Ge-C," Proceedings of the Third International Conference on CVD, Salt Lake City, Utah (1972).
14. E. Pickering, W. J. Lackey, and S. Crain, "Thermodynamic Modeling of the Ti-Si-C-H-Cl-Ar System to Determine Optimum Conditions for Vapor Deposition of Ti_3SiC_2," *Ceramic Engineering Science Proceedings*, 19[4], 541-552 (1998).
15. C. Racault, F. Langlais, and C. Bernard, "On the Chemical Vapor Deposition of Ti_3SiC_2 from $TiCl_4$-$SiCl_4CH_4$-H_2 Gas Mixture: Part 1, A Thermodynamic Approach," Journal of Materials Science, 29[1], 5023-5040 (1994).
16. Elliot Pickering, W. Jack Lackey, and Steven Crain, "Chemical Vapor Deposition of Ti_3SiC_2," submitted for publication in Advanced Materials, 1999.

Publications Resulting from this Research

1. K. A. Appiah, Z. L. Wang, and W. J. Lackey, "Characterization of Interfaces in C Fiber-Reinforced Laminated C-SiC Matrix Composites," Carbon, Accepted 1999.
2. K. A. Appiah, Z. L. Wang, and W. J. Lackey, "Growth and Texture of Polycrystalline SiC on Graphite During Forced-Flow Thermal Gradient Chemical Vapor Infiltration (FCVI)," Microscopy and Microanalysis, In Press 1999.
3. K. A. Appiah, Z. L. Wang, and W. J. Lackey, "Texturing of Polycrystalline SiC on Graphite Carbon Fibers," Applied Physics Letters, In Preparation (1999).
4. Elliot Pickering, W. Jack Lackey, and Steven Crain, "Chemical Vapor Deposition Ti_3SiC_2, Submitted for publication in Advanced Materials, 1999.
5. E. Pickering, W. J. Lackey, and S. Crain, "Microstructure of Ti_3SiC_2 Coatings Synthesized by CVD," Ceramic Transactions, 96 39-50, 1999.
6. K. A. Appiah, Z. L. Wang, and W. J. Lackey, "Effects of Deposition Temperature on Microstructure of Laminated (SiC-C) Matrix Composites," Journal Materials Science, Submitted 1998.
7. K. A. Appiah, Z. L. Wang, and W. J. Lackey, "Microstructural Characterization of Carbon Fiber-Reinforced Laminated Matrix Composites of Silicon Carbide and Carbon," Microscopy and Microanalysis, Vol. 4, Suppl. 2, 568-569, 1998.
8. Elliott Pickering, "Chemical Vapor Deposition of Ti_3SiC_2," Master of Science Thesis in Materials Science and Engineering, Georgia Institute of Technology, Atlanta, Georgia USA, June 1998.
9. E. Pickering, W. J. Lackey, and S. Crain, "Thermodynamic Modeling of the Ti-Si-C-H-Cl-Ar System to Determine Optimum Conditions for Chemical Vapor Deposition of Ti_3SiC_2," Ceramic Engineering Science Proceedings, 19(4) 541-552, 1998.
10. W. Jack Lackey, H. C. King, III, M. A. Miller and K. L. More, "Laminated Matrix Composites Produced by CVI," Invited Paper, Innovative Processing and Synthesis of Ceramics, Glasses and Composites, Ceramic Transactions, The American Ceramic

Society, Westerville, Ohio, , N. P. Bansal, K. V. Logan, and J. P. Singh, eds., 85 275-293, 1997.

11. W. J. Lackey, S. Vaidyaraman, and K. L. More, "Laminated C-SiC Matrix Composites Produced by CVI," Journal of the American Ceramic Society, 80(1) 113-116, 1997.
12. W. J. Lackey, S. Vaidyaraman, and K. L. More, "Laminated Matrix Composites - A New Class of Materials," Ceramic Engineering Science Proceedings, 17(4B) 166-173, 1996.

journal

J. Am. Ceram. Soc., 80 [1] 113-16 (1997)

Laminated C-SiC Matrix Composites Produced by CVI

W. Jack Lackey*

Georgia Tech Research Institute, Georgia Institute of Technology, Atlanta, Georgia 30332

Sundar Vaidyaraman†

School of Chemical Engineering, Georgia Institute of Technology, Atlanta, Georgia 30332

Karren L. More*

Oak Ridge National Laboratory, Oak Ridge, Tennessee 37830

A new type of composite, which consists of a reinforcement phase plus a matrix composed of many alternate thin layers of two different materials, has been prepared. CVI appears to be an appropriate process for the fabrication of this class of materials. We have successfully fabricated such a composite using the forced flow–thermal gradient CVI process. A carbon fibrous preform was infiltrated with alternate layers of C and SiC having thicknesses of 0.01 to 0.5 μm. For a fixed cycle time, layer thicknesses increased with distance from the fiber surface. Crack deflection patterns indicate that the laminated matrix may contribute to mechanical toughness.

I. Introduction

It is well known that ceramics have desirable properties, such as light weight, high stiffness, corrosion/wear resistance, and strength retention at high temperatures. However, their brittleness limits their use in most structural applications. Metals have excellent toughness but typically suffer from loss of strength at high temperatures, excessive creep, and high density. These shortcomings have been partially overcome for ceramics and metals using fibers or whiskers as reinforcement and also in metals using platelets and particulates. For example, the toughness of SiC and carbon have been improved by reinforcement with SiC and carbon fibers.[1,2] Also, SiC fibers or platelets have been used to reinforce Ti, Al, and other metals.[2] In these prior examples, the matrix was either single phase or contained a dispersed phase.[3]

It is also well known that the mechanical properties of structures can be enhanced by using alternate layers of two materials. Examples of such laminated materials include Ni/Cu, Fe/Cu, ZrO_2/Al_2O_3, SiC/C, TiC/TiN, TiC/TiB_2, TiC/Ni, Al_2O_3/Nb, and many others.[4–9] Many of these systems, particularly those with very thin layers which reveal the superlattice structure, have been reviewed by Barnett.[10] For most systems, it is clear that the mechanical and tribological properties improve significantly as layer thicknesses decrease, often rapidly as the layer thickness approaches ~0.02 μm.

The present work was undertaken to combine the advantages of fiber or particulate reinforcement and laminated structures. The resulting composite would have a reinforcement phase and a laminated matrix. It is suggested that this new class of composites be termed "Laminated Matrix Composites" (LMC). Laminated structures are typically fabricated by stacking foils, followed by hot pressing or diffusion bonding, various coating processes, sedimentation, centrifuging, and electrophoresis. These processes, with the exception of CVI, do not readily lend themselves to the infiltration of fibrous or particulate preforms, although Whitehead *et al.*[11] have prepared a thick-layered alumina–zirconia matrix by electrophoresis. Furthermore, several of the processes are not applicable to submicrometer thick layers, because of difficulties with handling or limitations on the size of the constituents. However, using CVI, a porous preform can be infiltrated with a laminated matrix by periodically changing the reagent stream from one type of precursor to another. In this way, many thin matrix layers may be easily deposited. Both CVD and CVI have been used to make multilayered fiber–matrix interface coatings[12–14] and oxidation protection coatings for carbon and other composites.[15,16] Naslain *et al.*[17] have used CVI to deposit what they refer to as a hybrid matrix where the first portion of the infiltration process is accomplished using one material and the final infiltration step utilizes a second material. Similarly, we and others have prepared fiber-reinforced composites where the matrix was subdivided into three to five layers.[18–22] Polymeric precursors, pitch, or CVI were used to synthesize either a C–SiC or BN–SiC matrix. Steffier and Shinavski[23] have deposited a layered C–SiC matrix and subsequently removed the carbon layers by oxidation, thus obtaining a "layered" SiC matrix.

The approach of the prior work consisted of repeating the fiber–matrix interface coating periodically throughout the matrix. That is, the vast majority of the matrix consisted of one phase, say SiC, which was partitioned into up to five thick layers by thin layers of the interface materials, i.e., carbon or BN.

The present work was undertaken with the goal of preparing a fiber-reinforced laminated matrix composite where the layers were significantly thinner than in the prior work. Accordingly, up to 80 layers as thin as 0.01 μm were used with the view that the thinner layers, as previously discussed, would enhance the mechanical properties. The two components chosen for the matrix were C and SiC with carbon fibers as the reinforcement phase. This system is of interest since the components are light, chemically compatible, and obtainable via CVI. Further, the anisotropic structure of carbon permits debonding and thus the potential for arresting the propagation of cracks, i.e., toughening.

II. Experimental Details

Laminated matrix composites (LMC) in the shape of right circular disks were fabricated using the forced flow-thermal

Roger Naslain—contributing editor

Manuscript No. 192405. Received August 7, 1995; approved July 10, 1996.
Supported by the Air Force Office of Scientific Research, the Georgia Institute of Technology, and the U.S. Department of Energy through the High Temperature Materials Laboratory User Program, under Contract No. 96OR22464 with Lockheed Martin Energy Research Corporation.
*Member, American Ceramic Society.
†Current address: Aircraft Braking Systems Corporation, Akron, OH.

Table I. Processing Conditions for Laminated Matrix Composites

Run No.	Preform type	Temperature of preform bottom (°C)	Carbon deposition time per cycle (min)	SiC deposition time per cycle (min)
L-1	3	910–950	5	5
L-2	3	915–954		
L-3	2	900–961	5	5
L-5	3	910–959	5	10
L-6	2	900–967		

gradient CVI process. In this process, a pressure gradient forces the reagent stream to flow through a preform which is subjected to a temperature gradient. The details of the equipment and general experimental procedure have been explained elsewhere.[24] Briefly, the preforms consisted of 40 layers of T-300 plain weave carbon cloth, 4.8 cm in diameter, oriented at 0° and 90°. These layers were stacked in a graphite preform holder and lightly compacted, giving a height of ~0.8 cm. Two types of preform holders, namely, type 2 and 3, which are described in a prior publication,[24] were used. The type 2 and 3 preform holders extended 5.1 and 7.6 cm above the gas injector, respectively. The height of the preform holder influences the temperature and the temperature gradient through the preform. The temperature differences between the hot and cold sides for the type 2 and 3 preform holders were ~350° and ~150°C, respectively.

The operating conditions for the infiltration experiments are given in Table I. A thin carbon interface was deposited before the deposition of the laminated matrix. The interface was deposited by flowing 40 cm^3/min of methane and 160 cm^3/min of hydrogen through the preform for 20 min. The temperature of the bottom of the preform during the interface deposition was ~975°C. This step was followed by deposition of C and SiC, alternately. Carbon was deposited from a reagent mixture containing 50% propylene–50% hydrogen, and the total flow rate was 400 cm^3/min. The SiC layers were deposited using 50 cm^3/min of methyltrichlorosilane (MTS) and 500 cm^3/min of hydrogen. The deposition time for each laminate layer was 5 min except for L-5, where each SiC layer was deposited for 10 min. Two infiltration runs (L-2 and -6) were conducted using only a carbon matrix for the purpose of comparison with the LMCs.

The temperature of the bottom of the preform during the course of depositing the laminated matrix fluctuated between 900° and 961°C. This temperature variation was caused by changing the reagent stream, thereby altering the thermal conductivity of the gas between the water-cooled gas injector and the preform. The thermal conductivity of the propylene/hydrogen mixture was lower than that of the MTS/hydrogen mixture for the concentrations used in the present work. Consequently, the temperature increased when the propylene/hydrogen mixture was used as the reagent, and the temperature decreased when the reagent was changed to MTS/hydrogen. About 60 s elapsed between ending the deposition of one layer and starting the deposition of the next layer. During this interval, hydrogen was flowed through the composite.

The apparent volume of the composite was determined using Archimedes' principle with methanol (ρ = 0.79 g/cm^3). The open-pore volume was calculated by weighing the composite saturated with methanol. These two values were added to obtain the bulk volume. To calculate total porosity it was assumed that the densities of the deposited carbon and SiC were 1.9 and 3.2 g/cm^3, respectively, and that the volume of carbon deposited was twice that of the SiC deposited. This latter assumption is an approximation based on observed microstructures.

An entire cross section of each composite disk was mounted in epoxy and polished. The polished sections were observed via scanning electron microscopy to permit observation of the composite microstructure. Several samples were fractured, using flexure, to observe the propagation of cracks. Transmission electron microscopy was used to more clearly observe the thinner layers and to determine the phases deposited.

III. Results

The objective of this work was realized; laminated matrix composites containing numerous very thin layers were successfully prepared. The infiltration time, density, and porosity of the laminated matrix composites (L-1, -3, and -5), and carbon matrix composites (L-2 and -6) used as controls, are given in Table II. The infiltration time for the laminated composites was 4.5–8 h versus ~4 h for the carbon matrix composites; apparently, this is the result of SiC deposition being slower than carbon deposition for the conditions used here. The open porosity of the laminated matrix and that of the carbon matrix samples are similar, but the closed porosity values are higher for the laminated matrix composites. This indicates that the conditions used for SiC infiltration require adjustment in order to achieve similar levels of closed porosity.

Scanning electron microscopy showed that the desired laminated matrix composites were achieved in each case (Figs. 1–3). Both the C and SiC layers were generally continuous with the exception of the first few layers in sample L-3. Transmission electron microscopy and electron diffraction verified that the deposits were turbostratic carbon and crystalline SiC, as expected. The number of layers at a given location depended on the space between the fibers. In a cloth layup, as used in the present work, the distance between the fibers within a tow was 2–3 μm (micropores), and the distance between the tows was 50–100 μm (macropores). The tows became densified early in the infiltration process, and most of the infiltration time was spent on filling the macropores found between the cloth layers and tows within a cloth.[21] Hence, not all layers were observed within a tow (Fig. 3). However, all the layers were observed in the matrix deposited within the macropores (Fig. 2).

As shown in Figs. 1–3, layers of C and SiC <0.5 μm in thickness were achieved. The thickness of the deposited layers generally increased with increasing distance from the fiber surface during the deposition process. The thickness of the initial layers was as small as 0.01 μm and increased to ~0.5 μm near the end of the deposition process. The increase in the deposition rate, i.e., layer thickness, with infiltration time was caused by

Table II. Properties of the Infiltrated Composites

Run No.	Fiber content (vol%)	Total No. of cycles	Infiltration time (h)	Weight gain (g)	Bulk density (g/cm^3)	Total porosity (%)	Open porosity (%)
L-1	50.6	40	6.67	12.90	1.672	16.4	5.94
L-2	49.0		4.25	11.74	1.658	9.2	4.97
L-3	56.7	27	4.50	14.74	1.700	13.7	5.56
L-5	51.8	32	8.00	12.88	1.647	17.7	8.90
L-6	50.8		3.60	13.11	1.692	7.6	7.57

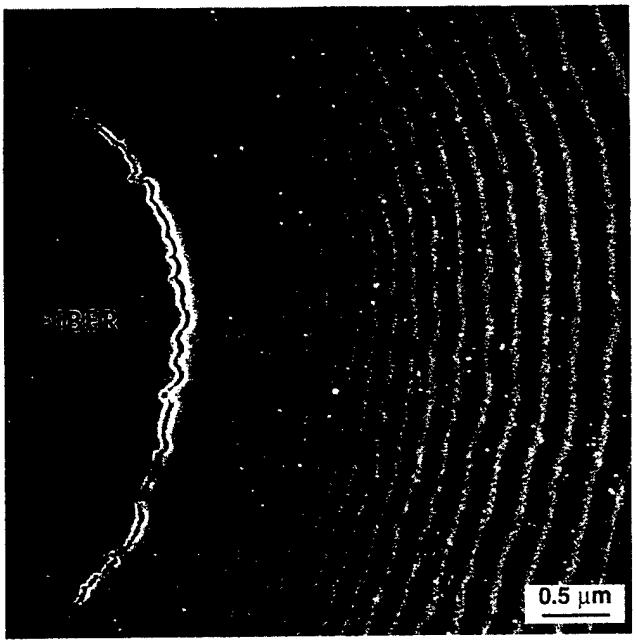

Fig. 1. Laminated matrix composite prepared by FCVI showing carbon fiber and alternating layers of carbon (dark) and SiC (light). Sample L-1.

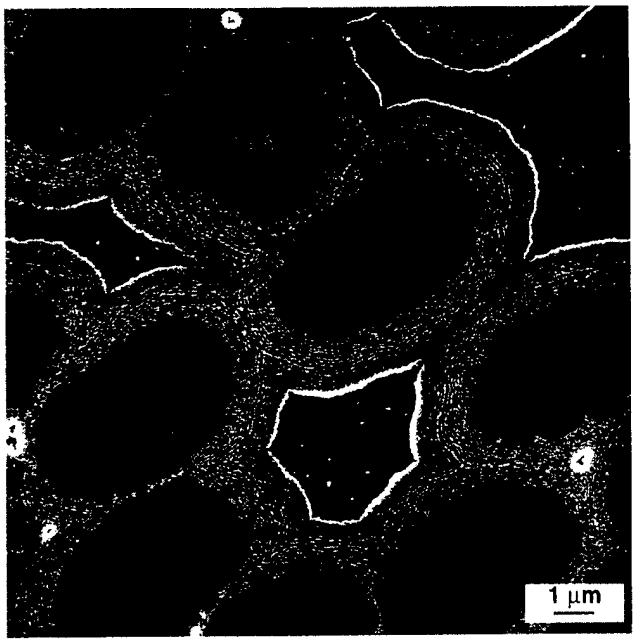

Fig. 3. The number of laminate layers between individual fibers depends on the distance between fibers. Sample L-5.

reduction of reagent depletion during the infiltration process. The term "reagent depletion" refers to the reduction in concentration of the reagent as the process gas stream traverses the preform. Initially the reagent depletion was very high due to the high surface area of the preform, but since densification isolates an ever-increasing number of tows, the surface area of the preform gradually reduces. This reduction in surface area, in turn, reduces reagent depletion and thereby leads to the observed increase in layer thickness with time.

Several samples were deliberately fractured in order to observe, via SEM, the crack path. As shown in Fig. 4, evidence that the laminate layers offer resistance to crack propagation was seen. The crack shown here does not propagate in a straight line, but instead follows a tortuous path with jogs occurring from one laminate layer to an adjacent layer. Typical debonding at the fiber–matrix interface (not shown) was also observed. While these results are encouraging, extensive mechanical testing will be required to determine if the laminated matrix does indeed enhance composite toughness.

IV. Discussion

Considerable experimental investigation and/or modeling of the fracture behavior of laminated matrix composites will likely be required in order to determine optimum material combinations and layer thicknesses for maximizing mechanical performance. Questions to be answered include identifying the preferred relative elastic moduli and strengths for the matrix materials, the modulus of the matrix compared to that of the

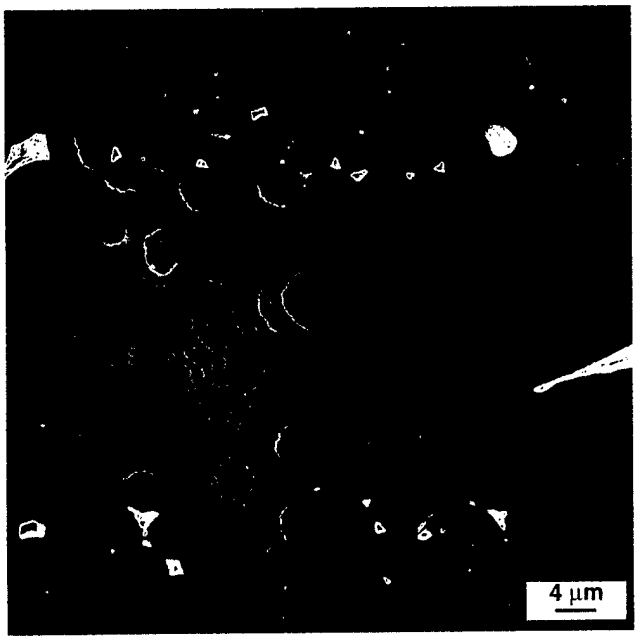

Fig. 2. Laminated matrix fills region between layers of cloth. Sample L-3.

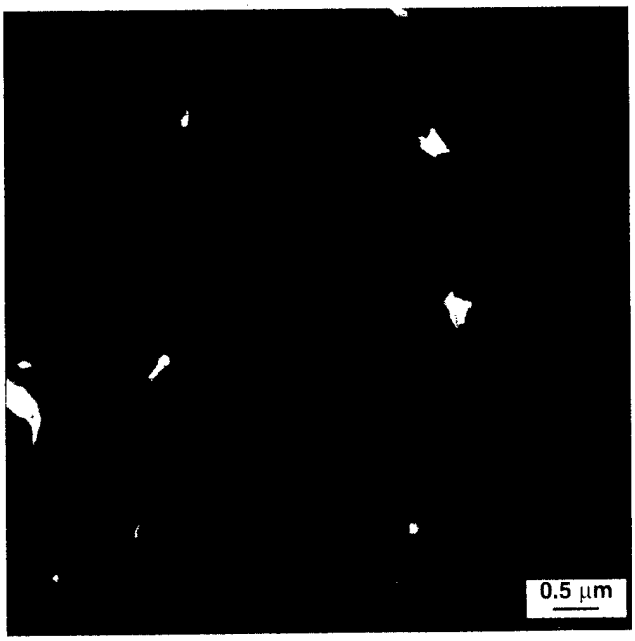

Fig. 4. Deliberate fracture showing tortuous crack path in the laminated matrix. Sample L-1-M-3.

reinforcement, and should be layers the ceramic, metallic, or one ceramic and one metallic. Also, it remains to be determined whether the laminate layers should be of equal thickness or should one type layer be thicker? Should a given type layer be of uniform thickness, or should the layers vary in thickness with distance from the reinforcement phase?

The laminated matrix composite concept offers a number of interesting options for improving performance and lowering costs. For example, if the multiple interfaces within the laminated matrix are effective in retarding crack propagation, that is, increasing toughness, then it may be possible to use particles or platelets, rather than fibers, as the reinforcement phase. If this is shown to be possible, then appreciable reduction in composite costs would result. Particles of SiC are commercially available in a variety of sizes for $1–2/lb compared to $300/lb for Nicalon SiC fiber. It may be that readily cleaved oxides, such as the β″-aluminas, magnetoplumbites, or monazite, may be appropriate materials for use as the reinforcement or as one of the matrix layers.

V. Summary

Laminated matrix composites containing fiber reinforcement and a matrix composed of alternate layers of C and SiC were successfully prepared using the forced-flow–thermal-gradient CVI process. Layer thicknesses were in the range 0.01–0.5 μm and increased with distance from the fiber surface because of a reduction of surface area as densification progressed. Nonlinear crack paths in the matrix indicated that lamination may enhance mechanical toughness.

Acknowledgments: We appreciate the guidance of Dr. Alexander Pechenik of the Air Force Office of Scientific Research. The assistance of Michael Miller, Regina Richards, and seven diligent undergraduate mechanical engineering students who performed most of the experimentation is appreciated. We also appreciate typing and editing of the original manuscript by Virginia Myers and Joey Goddard, respectively.

References

[1]W. J. Lackey and T. L. Starr, "Fabrication of Fiber-Reinforced Ceramic Composites by Chemical Vapor Infiltration: Processing, Structure and Properties"; pp. 397–450 in *Fiber Reinforced Composites*. Edited by K. S. Mazdiyasni. Noyes Publications, Park Ridge, NJ, 1990.

[2]M. R. Piggott, *Load Bearing Fibre Composites*. Pergamon Press, New York, 1980.

[3]S. R. Goujard, L. Vandenbulcke, J. Rey, J.-L. Charvet, and H. Tawil, "Process for the Manufacture of a Refractory Composite Material Protected against Corrosion," U.S. Pat. No. 5 246 736, September 21, 1993.

[4]W. J. Clegg, K. Kendall, N. M. Alford, D. Birchall, and T. W. Burton, "A Simple Way to Make Tough Ceramics," *Nature (London)*, **347**, 455–57 (1990).

[5]R. F. Bunshah, R. Nimmagadda, H. J. Doerr, B. A. Movchan, N. I. Grechanuk, and E. V. Dabizha, "Structure and Property Relationships in Microlaminate Ni–Cu and Fe–Cu Condensates," *Thin Solid Films*, **72**, 261–75 (1980).

[6]D. B. Marshall, J. J. Ratto, and F. F. Lange, "Enhanced Fracture Toughness in Layered Microcomposites of Ce–ZrO_2 and Al_2O_3," *J. Am. Ceram. Soc.*, **74** [12] 2979–87 (1991).

[7]M. Ignat, M. Nadal, C. Bernard, M. Ducarrioir, and F. Teyssandier, "Mechanical Response and Rupture Mode of SiC/C Lamellar Composites," *J. Phys.*, **50**, C5–259 (1989).

[8]A. J. Phillipps, W. J. Clegg, and T. W. Clyne, "The Correlation of Interfacial and Macroscopic Toughness in SiC Laminates," *Composites*, **24** [2] 166–76 (1993).

[9]J. T. Beals and V. C. Nardone, "Tensile Behavior of a Niobium/Alumina Composite Laminate," *J. Mater. Sci.*, **29**, 2526–30 (1994).

[10]S. A. Barnett, "Deposition and Mechanical Properties of Superlattice Thin Films"; pp. 1–77 in *Physics of Thin Films*, Vol. 17. Edited by M. H. Francombe and J. L. Vossen. Academic Press, New York, 1993.

[11]M. Whitehead, P. Sarkar, and P. S. Nicholson, "Non-Planar Al_2O_3/YPSZ Laminates by Electrophoretic Deposition Using Al_2O_3 Fibre Electrodes," *Ceram. Eng. Sci. Proc.*, **15** [5] 1110–17 (1994).

[12]T. Huynh and W. E. Bustamante, "Non-Oxidizing Interface (NOI) for Ceramic Matrix Composites Processed by CVI Technique"; presented at 17th Annual Conference on Composites, Materials, and Structures (Restricted Session), Cocoa Beach, FL, January 14, 1993.

[13]C. Droillard, J. Lamon, and X. Bourrat, "Strong Interface in CMCs, Condition for Efficient Multilayered Interphases"; in Proceedings of the Fall Meeting of the Materials Research Society, Vol. 325 (Boston, MA, November, 1994). Materials Research Society, Pittsburgh, PA, in press.

[14]C. Droillard, "2D-SiC/SiC CVI Composite with a $(C\text{-}SiC)_n$ Multilayered Interphase: Processing, Microstructure and Tensile Behavior at Room Temperature"; Thesis. University of Bordeaux, France, June, 1993.

[15]J. E. Sheehan, "High-Temperature Coatings on Carbon Fibers and C–C Composites"; pp. 223–66 in *Carbon–Carbon Materials and Composites*. Edited by J. D. Buckley and D. D. Edie. Noyes Publications, Park Ridge, NJ, 1993.

[16]L. Vandenbulcke, S. Goujard, H. Tawil; and J.-C. Cavalier, "Method of Providing Antioxidation Protection for a Composite Material Containing Carbon, and a Material Protected Thereby," U.S. Pat. No. 5 194 330, March 16, 1993.

[17]R. Naslain, J. Y. Rossignol, P. Hagenmuller, F. Christin, L. Heraud, and J. J. Choury, "Synthesis and Properties of New Composite Materials for High Temperature Applications Based on Carbon Fibers and C–SiC or C–TiC Hybrid Matrices," *Rev. Chim. Miner.*, **18**, 544–64 (1981).

[18]R. P. Boisvert, "Ceramic Matrix Composites via Organometallic Precursors"; M.S. Thesis. Rensselaer Polytechnic Institute, Troy, NY, May, 1988.

[19]R. J. Diefendorf and R. P. Boisvert, "Processing of Polymeric Precursor, Ceramic Matrix Composites," *Mater. Res. Soc. Symp. Proc.*, **120**, 157–62 (1988).

[20]L. Heraud, R. Naslain, and J. M. Quenisset, "Method for Producing a Ceramic Matrix Composite Material Having Improved Toughness," U.S. Pat. No. 5 0079 039, January 7, 1992.

[21]W. J. Lackey, S. Vaidyaraman, G. B. Freeman, and P. K. Agrawal, "Technique for Monitoring the Densification during CVI Processing," *J. Am. Ceram. Soc.*, **78** [4] 1131–33 (1995).

[22]R. P. Boisvert, "A Thermodynamic and Kinetic Study of the Deposition of SiC from Various Precursor Systems with Application to the Preparation of Lamellar-Matrix/Continuous Fiber-Reinforced Composites"; Ph.D. Thesis. Rensselaer Polytechnic Institute, Troy, NY, December 1995.

[23]W. S. Steffier and R. J. Shinavski, "Toughened SiC Fiber-Reinforced Ceramics via Multiple Unbonded SiC Matrix Layers"; presented at the 19th Annual Conference on Composites and Advanced Ceramics, Cocoa Beach, FL, January 10, 1995.

[24]S. Vaidyaraman, W. J. Lackey, G. B. Freeman, P. K. Agrawal, and M. D. Langman, "Fabrication of Carbon–Carbon by Forced Flow-Thermal Gradient Chemical Vapor Infiltration," *J. Mater. Res.*, **10** [6] 1469–77 (1995). □

Chemical Vapor Deposition of Ti_3SiC_2

(Submitted for publication in Advanced Materials, 1999)

Elliot Pickering*, W. Jack Lackey**, Steven Crain*

*School of Materials Science and Engineering

**G.W. Woodruff School of Mechanical Engineering

Georgia Institute of Technology

Atlanta, Georgia 30332

ABSTRACT

Thermodynamic calculations and experiments were performed to better understand the CVD of Ti_3SiC_2. The computer program SOLGASMIX-PV was used to calculate deposition diagrams for the $TiCl_4$-$SiCl_4$-CCl_4-H_2 reagent system. The effects of hydrogen to reagent concentration, temperature, and pressure were explored with a "box" type study, surrounding a middle condition of 1300K, 760 kPa, and a hydrogen to reagent concentration ratio of 20:1. Results suggest that Ti_3SiC_2 prefers to deposit at lower hydrogen to reagent concentrations, lower temperatures, and higher pressures. An experimental study of the CVD of Ti_3SiC_2 was also conducted revealing important morphological details about deposited Ti_3SiC_2. Deposits showed a complicated microstructure consisting of various combinations of Ti_3SiC_2, TiC, and $TiSi_2$. The preferred orientation of Ti_3SiC_2 basal planes was shown to be perpendicular to the substrate, with the degree of orientation and other microstructural characteristics dependent on temperature.

KEY WORDS: Ti_3SiC_2, Thermodynamic Modeling, CVD, Microstructure, Composites

INTRODUCTION

The integration of fiber-matrix ceramic interface coatings like carbon (graphite) and hexagonal BN have resulted in improved fracture toughness and lifetime to failure for fiber-reinforced composites at low temperature.[1-3] These coatings are typically deposited by chemical vapor deposition (CVD). The success of carbon and BN was attributed to their crystal structures. Weakly bonded basal planes, when oriented parallel to the fiber reinforcement, served to deflect cracks propagating through the matrix, thus preserving the integrity of the fibers. Fiber pullout and fiber bridging mechanisms are enabled, which lead to improved mechanical properties. Unfortunately, these effects are subdued at high temperature due to oxidation susceptibility. In response, a tremendous effort by the ceramic community was launched in order to identify and synthesize high temperature, oxidation resistant alternatives. To date, oxide compounds in the monazite, magnetoplumbite, and other systems have received extensive attention.[4-6] The exploration of Ti_3SiC_2 as a fiber-matrix interface is a natural extension of this work because it has better resistance to oxidation than carbon and BN, current interface coating.[7,8]

Investigation of Ti_3SiC_2 has accelerated in recent years as its properties suggested a host of possible applications. Its layered crystal structure, high temperature ductility, and parabolic oxidation resistance suggest it may be appropriate for fiber-matrix interface

applications in ceramic matrix composites. It may also be useful as the matrix or as a layer material in laminated matrix composites.[9] The resulting "laminated matrix composite" might have enhanced fracture toughness compared to a composite containing a monolithic matrix.

The FCVI process often involves deposition over a range of temperatures, pressures, and reagent concentrations. Therefore, in order to deposit Ti_3SiC_2 by the forced flow chemical vapor infiltration (FCVI) process[9], a thorough understanding of the CVD of Ti_3SiC_2 must be established, including the thermodynamics and kinetics of the reaction, as well as the extent of the Ti_3SiC_2 deposition field. Since 1972 only three groups have previously published on the CVD of Ti_3SiC_2.[10-12] This knowledge base is insufficient to permit the application of the FCVI process to Ti_3SiC_2. The goal of the present work, was to further that understanding by performing thermodynamic modeling of the $TiCl_4$-$SiCl_4$-CCl_4-H_2 reagent system and conducting an experimental CVD study. It is hoped that the resulting data from both modeling and experimentation together may reveal important parameters necessary for the successful CVD and CVI of Ti_3SiC_2 in future work.

PREVIOUS CVD OF Ti_3SiC_2

Prior CVD synthesis of Ti_3SiC_2 is summarized in Figure 1.[10-12] Reagent compositions are shown on a ternary deposition diagram, along with the deposition temperature, pressure and hydrogen dilution used during these CVD studies. Nickl et al.[10] completed

the most comprehensive study of the $TiCl_4$-$SiCl_4$-CCl_4-H_2 deposition system in 1972, experimentally determining the entire range of the ternary deposition diagram with more than 100 experiments. Nickl et al.[10] report polycrystalline layers of Ti_3SiC_2 below 1200° C and single crystal, hexagonal plates above 1300° C. Goto and Hirari[11] reported the next successful attempt at single phase Ti_3SiC_2 deposition in 1987. Like Nickl et al., they prepared thick films of monolithic Ti_3SiC_2 using the $TiCl_4$-$SiCl_4$-CCl_4-H_2 reagent system. Deposition rates were reported at 200 μm/h. The final group to publish on the CVD of Ti_3SiC_2 was Racault et al.[12] in 1994. They used the $TiCl_4$-$SiCl_4$-CH_4-H_2 reagent system, citing the reduced thermal stability of CH_4 over CCl_4. Their work demonstrated the importance of hydrogen dilution, a parameter they called α. This was defined as the ratio of hydrogen to the total amount of Si-Ti-C containing reagents, or $\alpha = X_{H2} / (X_{TiCl4} + X_{SiCl4} + X_{CH4})$. This work failed to produce single phase Ti_3SiC_2 under any conditions studied, but instead Ti_3SiC_2 was co-deposited with $TiSi_2$ or Ti_5Si_3 and small amounts SiC and TiC. Our objectives were to explore by thermodynamic calculations and CVD experiments wider ranges of processing conditions that should be useful for FCVI. Film microstructures determined by XRD and SEM/EDS were also closely correlated with processing conditions.

THERMODYNAMIC MODELING

In the present work, deposition diagrams were calculated for the $TiCl_4$-$SiCl_4$-CCl_4-H_2 reagent system using the SOLGASMIX-PV computer program.[13-15] SOLGASMIX-PV

computed equilibrium conditions for a particular chemical system given input quantities of reactants, temperature and pressure, a list of possible products (gases, liquids and solids), and corresponding enthalpy and entropy for each chemical species considered. The computer program follows several iterations until the free energy of the entire mixture is minimized. A total of 65 species were considered, 17 solids and 48 gases. There were no liquids suitable for consideration in this system. The thermodynamic data used have been previously published.[16] All thermodynamic data were taken at 1300K from the JANAF tables,[17] except data for the titanium silicides, Ti_3SiC_2, and $Ti_5Si_3C_x$. Titanium silicide data were obtained from Kubaschewski and Evans[18] and Engqvist et al.[19] and Vahlas et al.[20] These papers give enthalpy, entropy, and heat capacity values for titanium silicides at 298 K. These data were applied to Kirchhoff's Law to obtain enthalpy and entropy values at 1300K. Thermodynamic data for the two ternary phases in the Ti-Si-C system, Ti_3SiC_2 and $Ti_5Si_3C_x$, were obtained from Racault et al[21] and Sambasivan.[22] These papers, based on our computerized literature search, are the only source of thermodynamic data for these ternary phases. The only prior effort at thermodynamic modeling of the CVD of Ti_3SiC_2 is the work of Racault et al.[21]

Simulated deposition conditions (temperature, pressure, and hydrogen to reagent concentration ratio) for which deposition diagrams were calculated were chosen using a "box" type design. The middle condition of the study was 1300K, 101 kPa, and a hydrogen to reagent concentration ratio of 20:1. Temperature was varied from 1100 to 1500K. Pressure was varied from 40.0 to 203 kPa. The α parameter was varied from 10:1 to 30:1. In all, seven deposition diagrams were calculated in order to study the effects of these variables. Unlike the work for Racault et al.,[21] all calculations were

based on the reagent system $TiCl_4$-$SiCl_4$-CCl_4-H_2. In order to be complete, calculations were performed over the entire range of the phase diagram. SOLGASMIX-PV was used to perform a calculation at every 5% interval across the ternary for a total of 231 calculations per diagram. This permits construction of approximate ternary deposition diagrams but does not locate all small phase fields, and thus portions of the diagram appear to violate the phase rule.

Calculated Deposition Diagrams

The deposition diagram for the middle condition of the study (1300K, 101 kPa, 20:1 α parameter) is shown in Figure 2. In addition to showing the location of each phase field, mole ratio contours are included around the single phase field for Ti_3SiC_2. These contours can be interpreted as the mole percent of Ti_3SiC_2 in the total deposit. The edges of the single phase field can be considered the 100% contour. Moving outward, the percentage of deposited Ti_3SiC_2 drops as other phases are also formed. The 80% and 50% mole ratio contours are shown for all deposition diagrams. To the left of the Ti_3SiC_2 single phase field is a two phase field consisting of Ti_3SiC_2 + $Ti_5Si_3C_x$. Above and to the right is the Ti_3SiC_2 + SiC phase field, while below and to the right is Ti_3SiC_2 + C. Located between the latter two phase fields is a three phase field where Ti_3SiC_2 + SiC + C exist in equilibrium. Directly below the Ti_3SiC_2 single phase field is the two phase field Ti_3SiC_2 + TiC. There is also a three phase region consisting of Ti_3SiC_2 + C + TiC. In the $SiCl_4$-rich corner of the deposition diagram is a two phase field with SiC + $Ti_5Si_3C_x$ and a three phase field consisting of SiC + $Ti_5Si_3C_x$ + Ti_3SiC_2. The single phase region for $Ti_5Si_3C_x$ lies along the $TiCl_4$-$SiCl_4$ side of the diagram between 0-5% CCl_4. Other two phase regions exist between $Ti_5Si_3C_x$ and the titanium silicides

predicted on the edge of the diagram. The CCl_4-$SiCl_4$ edge of the diagram consists of separate single phase fields with C at one end and SiC at the other. Likewise TiC and C are shown along the CCl_4-$TiCl_4$ edge. With the exception of the 60 calculations along the edges, and a small region near the $SiCl_4$-rich side, Ti_3SiC_2 is predicted over the entire diagram.

Temperature Dependence

Temperature had the largest effect on Ti_3SiC_2 deposition. Temperature was varied from 1100K to 1300K (Figure 2) to 1500K (Figure 3), while pressure and the α parameter were kept at 101 kPa and 20:1, respectfully. The size of the single phase field for Ti_3SiC_2 increased dramatically at lower temperatures. This is a suspect result since Ti_3SiC_2 has been shown to be difficult to deposit as a single phase. It may indicate that either the thermodynamic data are in error or kinetics play a large role in the deposition of Ti_3SiC_2. However, the lowest deposition temperature in the literature was reported by Racault et al.[12] at 1373K, so no experimental work has been reported in this low temperature regime. Figure 3 stands in stark contrast. It suggests the Ti_3SiC_2 single phase field has shrunk significantly with a 400K increase in temperature. Because of the high temperature, the free energy of Ti_3SiC_2 is increased, rendering it less stable. This has the effect of reducing the single phase field to its smallest proportions of the entire study. At this point it is important to interject an important note about the following deposition diagrams. The single phase field for $Ti_5Si_3C_x$, and other two phase fields along the $SiCl_4$-$TiCl_4$ edge are not shown, for simplicity, in subsequent deposition diagrams.

Pressure Dependence

Pressure is an important parameter in forced-flow CVI. Reagent gasses are passed through a fiber preform and the matrix is deposited. As the preform densifies, some of the paths for flow of reagent gas become closed and an appreciable pressure gradient develops. The downstream side of the preform is typically maintained at the initial pressure while the upstream side of the preform is exposed to increasing back pressure. With this in mind, pressure was varied from 40.0 kPa (Figure 4), to 101 kPa (Figure 2) to 203 kPa, while temperature and the α parameter were held constant at 1300K and 20:1. The deposition diagrams show a trend toward a larger Ti_3SiC_2 single phase field as deposition pressure increased. Accordingly, Figure 4 shows a smaller single phase field for Ti_3SiC_2. The mole ratio contours are packed tightly on the left side as $Ti_5Si_3C_x$ begins to form. Like many of the deposition diagrams in this study, the single phase field tolerates a very wide range of $SiCl_4$ and $TiCl_4$ reagent concentrations, from 5-50% and 30-95%, respectfully. CCl_4 is the most restrictive reagent with compositions ranging from 20-35%. Previous work of Goto and Hirai, Nickl et al., and Racault et al. all confirm the narrow range of carbon compositions, coupled with a broader range of silicon and titanium compositions.[10-12] At 203 kPa, the single phase field was larger. It stretched farther upward toward richer silicon compositions, and farther to the right. This trend is encouraging for forced-flow CVI. CVD is rarely done at greater than atmospheric pressure, but the FCVI process might demand it. No previous experimental work has been done to verify this result.

Hydrogen to Reagent Ratio (α) Dependence

The results for the hydrogen concentration parameter, α, are surprising. It was varied from 10:1 to 20:1 to 30:1, while pressure and temperature were kept constant at 101 kPa and 1300K. The above ratios represent the number of moles of hydrogen for every mole of silicon, titanium, and carbon reagent. The deposition diagrams suggest that lower hydrogen concentrations support Ti_3SiC_2 deposition. This is contrary to the experimental work of Racault et al. who showed that increasing the hydrogen content enlarged the deposition range.[12]

EXPERIMENTAL PROCEDURE

Over 40 preliminary CVD experiments were performed in an effort to verify the results of previous authors. Conditions for these preliminary experiments covered a wide composition range from 5-30% CCl_4, 25-55% $TiCl_4$, and 25-60% $SiCl_4$, temperatures from 1000-1400°C, and hydrogen dilutions between 10-40. These initial experiments resulted in deposits containing only TiC or SiC. Only after increasing hydrogen dilution above 25 was Ti_3SiC_2 finally deposited. Based on these initial results, the following experimental study of the CVD of Ti_3SiC_2 was planned.

Four reagent compositions for the present study were chosen in the region of the deposition diagram in Figure 1 where previous CVD of Ti_3SiC_2 was achieved. The total hydrogen flow rate was kept constant at 2000 cm^3/min. This was done in order to limit variations in substrate temperature from experiment to experiment due the cooling

effect of flowing gas, and to minimize variation in the static gas boundary layer adjacent to the substrate. Because the hydrogen flow remained fixed while the flow of reagent varied, hydrogen dilution, α, varied from 42.1 to 32.0. The four reagent compositions were repeated at three different temperatures (1373, 1473, 1573K) for a total of 12 experiments. Pressure and run time were kept constant at 40.0 kPa and 150 minutes, respectfully. Table I shows run conditions listing the target flow rates, pressure, run time, α, and temperature for each experiment. The experiments were conducted in random order.

The deposition apparatus was a vertical, hot-walled reactor resistively heated with a graphite heating element. The heating element, reaction chamber, substrate stage, and substrate were graphite. The furnace was evacuated, leak checked, and back filled with argon before each experiment. The substrates were ATJ graphite cut to 20.5 x 5.1 x 58.5 mm, and suspended ~ 90 mm above the gas injector. The external reactor wall and gas injector were made of stainless steel and were water-cooled. Reactant gases were introduced through the gas injector, which in turn was supplied reagent gases through a series of 6.35 mm diameter stainless steel tubes and various 2 and 3-way valves. The tetrachloride reagents are liquids at room temperature and were vaporized using hydrogen as the carrier gas. Each vaporizer was equipped with a thermocouple and pressure gauge. Hydrogen flow to the vaporizers was adjusted according to the partial pressures of the reagents and controlled with MKS mass flow controllers. Excess hydrogen was routed through a separate line. Actual average reagent flow rates were determined by weight loss of the vaporizer from beginning to end of an experiment. Due to its very low vapor pressure, the $TiCl_4$ vaporizer was sometimes heated, and the stainless steel tubing

between it and the gas injector was always heated to avoid condensation in the lines. Mass flow controllers were calibrated through the calibration port before each experiment.

RESULTS

Table II gives the results from the study, listing run numbers with actual average flow rates, deposition temperature, deposited phases as determined by XRD and EDS, and coating thickness. Careful microscopy showed that Ti_3SiC_2 was never deposited as a single phase, even though XRD patterns for experiments at 1300°C suggest otherwise. SEM showed the microstructure of the films was quite complicated, involving co-deposition of Ti_3SiC_2 with TiC and small amounts of $TiSi_2$. Ti_3SiC_2 deposits were highly textured, with the basal planes preferentially oriented perpendicular to the substrate. Although XRD, SEM, and EDS showed significant amounts of Ti_3SiC_2 at 1100 and 1300°C, very little was deposited at 1200°C. Calculated flow rates show this study covered reagent compositions from 19-28% CCl_4, 30-45% $TiCl_4$ and 32-46% $SiCl_4$, and hydrogen dilution from 31-44. Ti_3SiC_2 was successfully deposited over most of this composition range. The films deposited at 1300°C showed large-grained, highly textured Ti_3SiC_2, while at 1100°C Ti_3SiC_2 was co-deposited with TiC. At 1200°C Ti_3SiC_2 deposited as a minor phase in a TiC matrix. Continuous planes of $TiSi_2$ parallel to the substrate surface appear at 1200 and 1100°C, but were believed to be caused by fluctuations in reagent composition through the course of the experiment.

Coating thickness varied from 99-215 μm. The following analysis shows that the character of the deposited films and the morphology of the Ti_3SiC_2 in the films was highly temperature dependent.

X-Ray Diffraction

Each of the films was subjected to XRD. Two XRD patterns from the study are shown in Figures 5 and 6. The peaks for each phase are labeled with the corresponding (hkl) values. Figure 5 is for run EP31, which was deposited at 1300°C. Only Ti_3SiC_2 peaks are evident; SEM showed some TiC was present, particularly at the coating-substrate interface. It is representative of two other high temperature experiments, EP24 and EP27. All show a great deal of preferred crystallographic orientation. Notice the (008) peak is totally missing in this scan, but according to the PDF card (40-1132) it should be the 100% peak. As further evidence of texture the (110) reflection is quite strong, which may be due the right angle orientation between (008) and (110) crystallographic planes. Another indication of preferred orientation is that the (107), (108), and (109) peaks are missing between 50-60° 2θ.

The pattern for EP23 is shown in Figure 6 This sample was deposited at 1100°C. It shows peaks for both Ti_3SiC_2 and TiC. The same preferred orientation is apparent in Ti_3SiC_2. The (008) peak is present, but clearly a weaker peak than (101), (104), (105) and others. The TiC peaks in these patterns do not show preferred orientation. Notice the TiC (220) peak directly overlaps the Ti_3SiC_2 (110) peak. Without knowing the

relative amounts of each phase, it is difficult to quantify how much of the peak intensity is due to which phase.

PDF Card Refinement

Several discrepancies were noted between the XRD patterns collected for this CVD study and the pattern for Ti_3SiC_2 recorded on the PDF card. Three peaks were consistently obtained during the course of this research that were not present on the card. Because these peaks are found in XRD patterns taken from samples prepared through different means, synthesized by different authors, and because they do not belong to other solids in the Ti-Si-C system, we concluded that the peaks belong to Ti_3SiC_2. The plane-spacing equation for hexagonal crystals was taken from Cullity.[23] Using this equation and the unit cell size for Ti_3SiC_2, it is possible to calculate for various values of (hkl) where additional peaks might occur. Excellent agreement between the calculated and observed d-spacings, as shown in Table III, strongly suggests that these three peaks are attributed to Ti_3SiC_2.

Preferred Orientation of Ti_3SiC_2

Irrespective of deposition temperature, preferred crystallographic orientation was observed in Ti_3SiC_2. In an effort to quantify this, the relative intensities of peaks in collected XRD patterns were compared to the relative intensities on the PDF cards. In the case where more than one phase was deposited, the relative intensity of each peak was normalized to the strongest peak for that phase. The relative intensities of deposited phases were divided by the relative intensity from the PDF card. The ratios can be interpreted in the following manner; ratios greater than one suggest the relative intensity

for that peak was greater than that on the PDF card, while a ratio less than one suggests the relative intensity for that peak was less than that on the PDF card. Consistent variation from a ratio of 1.0 was taken as evidence of texture in the coating. A ratio of 1.0 suggests that peaks intensity was consistent with the reported intensity.

Preferred orientation was seen in Ti_3SiC_2 peaks for every condition in the study. The ratio for the (008) peak was consistently less than 1.0 at all deposition temperatures, but 0.0 for the 1300°C experiments. Intensities for (101) and (104) peaks were greater than 1.0 for 1100 and 1200°C experiments, but less than 1.0 at 1300°C. This suggests the orientation of deposited Ti_3SiC_2 changed with temperature. It can be shown that the (110) peak also changed intensity with temperature, even though the ratios were not reliable due to the complication with the overlapping (220) TiC peak. At 1300°C, the intensity of this peak was 7.69 (the ratio for EP24, EP27, and EP31 are considered reliable because Ti_3SiC_2 was the only phase detected with XRD). At lower temperatures the intensity from this peak is significantly smaller, even though the deposition of TiC added intensity.

In order to further characterize the nature of preferred orientation in Ti_3SiC_2, the ratios were analyzed statistically using regression techniques. Linear regression of ratios for specific (hkl)s were explored with respect to temperature. Much of the scatter in the data was found for experiments performed at 1200°C. While the ratios were fairly consistent at 1100 and 1300°C, the four 1200°C experiments, EP14, EP15, EP19, and EP23, showed a wide range of variation from 0.0-1.0. This wide variation was probably due to

considerable weakness in Ti_3SiC_2 peak intensities for experiments performed at 1200°C. With the exception of EP14, virtually no Ti_3SiC_2 was detected by XRD in coatings deposited at this temperature. Because very few Ti_3SiC_2 peaks appear, and the intensity of these peaks was quite small, the (hkl) ratios for EP15, EP19, and EP23 were not included in the linear regression analysis on the premise that the Ti_3SiC_2 content of these coatings was too small to provide an accurate XRD pattern. EP14 showed many Ti_3SiC_2 peaks with significant intensities and so was retained as an example of the type of Ti_3SiC_2 preferred orientation found at 1200°C.

Table V shows the resulting statistical data from the linear regression of the (008), (101), and (104) ratios against temperature for the shortened data set. Included in the table are the constants for slope and intercept along with their corresponding significance levels and the R^2 value for each fit. The constants apply to the equation $Y = AX + B$, where Y is the (hkl) ratio, X is deposition temperature in degrees centigrade and A and B are constants. With respect to the (008) (hkl), the significance level for the slope constant, A, suggests 97% confidence that temperature influences crystallographic orientation of deposited Ti_3SiC_2.

Microstructure

Various microstructural characteristics are evident at different temperatures. Figure 7 shows a) the surface morphology, and b) the fractured cross section of Ti_3SiC_2 grown at 1300°C. The coating is highly oriented and characterized by large, plate-like grains oriented perpendicular to the substrate. This corroborates the preferred orientation seen with x-ray diffraction. Some regions of the coating appear to have the flat side of the

plate parallel to the fracture surface, while other regions appear to show the plate edge on. The surface morphology is similar in appearance to the Ti_3SiC_2 coating structure reported by Goto and Hirai.[11] The surface is an intricate pattern of grains, which are oriented in random directions. Taken together, these micrographs suggest that although the basal planes are oriented perpendicular to the substrate, there does not appear to be additional restrictions on the growth of Ti_3SiC_2. Figure 8 shows the a) surface morphology and b) fractured cross section of a coating grown at 1100°C. XRD suggests the sample is a mixture of Ti_3SiC_2 and TiC but individual phases and grains are not discernable at this magnification. Instead the coating cross section appears rather featureless. The surface appears to consist of small, nodule-like features growing on larger nodules. Compared with Figure 7, the microstructure is much finer. There is clearly a marked difference in deposition of highly oriented, large grained Ti_3SiC_2 at 1300°C and the fine grained co-deposition of TiC and Ti_3SiC_2 at 1100°C. Strangely, the 1200°C experiments did not yield significant amounts of Ti_3SiC_2.

Polished and etched $(1H_20:1HN0_3:1HF)$[24] cross sections revealed more details about the microstructure of these coatings. Figure 9 is a series of micrographs taken from experiments performed at 1100°C. Figure 9a shows the cross section of an over etched sample. The vertical bands running parallel to the substrate are the result of different etch rates on the different phases. EDS has shown these bands to be composed of Ti_3SiC_2, TiC and $TiSi_2$, again confirming data from XRD. Figure 9b was taken at higher magnification. Continuous layers of $TiSi_2$ appear early in the growth process, and are believed to be caused by fluctuations in reagent flow rates. As the carbon content of the

reagent mix becomes too low, $TiSi_2$ begins to form at the leading edge of the growing surface. The remainder of the coating consists of Ti_3SiC_2 and TiC growing simultaneously, as shown in Figure 9c. The layered crystal structure is apparent in the Ti_3SiC_2 grains, identified with EDS. Surrounding these grains are regions of TiC. The EDS spectrum from the TiC shows some silicon, but not enough to suggest Ti_3SiC_2. It is not clear whether the silicon signal is due to solid solubility of silicon in TiC or due to Ti_3SiC_2 grains hidden beneath the polished surface. Finally, Figure 9d also shows the microstructure of this two phase region at a lower magnification. The dark phase was identified with EDS as Ti_3SiC_2, while the lighter, matrix phase was identified as TiC.

Figure 10 shows a series of micrographs for 1300°C experiments. Figure 10a is the polished and etched cross section of one of these coatings. The layered structure growing perpendicular to the substrate in fan-like grains is readily apparent. A boundary layer appears between these grains and the substrate. EDS identified this boundary layer as TiC with a small amount of silicon. There is the possibility that the TiC layer formed as a result of reaction with the graphite substrate. A similar layer appears midway through the coating, parallel to the substrate, but much thinner. It is labeled the "intermittent layer". EDS shows this to be TiC as well. Figure 10b shows the interface between this TiC layer and Ti_3SiC_2 grains at high magnification. Notice how individual layers of the Ti_3SiC_2 grow directly into the TiC layer. The absence of a clear grain boundary between the TiC layer and Ti_3SiC_2 suggests a semi-coherent interface. Figure 10c shows the fan-like structure of Ti_3SiC_2 grains. Notice the cracks initiating in the "hilt" of the fan, and extending outward in a straight line, guided by individual layers of the grain. This demonstrates the crack deflecting properties of

layered Ti_3SiC_2. These grains appear to consist of a light and a dark phase, even though the layered appearance of the structure suggests Ti_3SiC_2, alone. EDS on individual layers showed the lighter phase too silicon deficient to be Ti_3SiC_2. Instead, the grain may consist of sandwiched layers of TiC and Ti_3SiC_2. This may correspond to the lamella TiC/Ti_3SiC_2 structure first described by Nickl et al.[10] Referring again to Figure 10a, the presence of TiC is further evidenced by a distinct demarcation approximately three fifths of the way through the coating, below which a great deal of the lighter phase, believed to be TiC, exists. Above this line, there is much less of the light phase. It is from this upper region that XRD data are collected, and perhaps one reason TiC is not seen with XRD. Figure 10d shows Ti_3SiC_2 grains in this region near the surface of the coating. The layered nature of the plate-like crystals is unmistakable, with some grains oriented edge on and some oriented flat to the field of view. EDS from these regions confirmed the presence of Ti_3SiC_2.

SUMMARY AND CONCLUSIONS

Thermodynamic modeling has shown that the extent of the Ti_3SiC_2 single-phase field is highly dependent on process conditions. Although there was minimal agreement between calculated results and experimental results, thermodynamics alone may not be sufficient to completely model the system. Instead, the disagreement suggested that kinetics might play an important part in the CVD of Ti_3SiC_2. Furthermore, calculated deposition diagrams represent the minimum free energy of the system, given sufficient time to react. At lower temperatures, it is possible that more time is needed to reach that minimum free

energy, while at higher temperatures the kinetics of the reaction may be sufficiently fast to reach equilibrium. Calculated deposition diagrams showed Ti_3SiC_2 preferred to deposit at lower temperatures, lower hydrogen dilution, and higher pressures. This study, to the best of our knowledge, was the most complete thermodynamic modeling of the $TiCl_4$-$SiCl_4$-CCl_4-H_2 reagent system to date.

The CVD experimental study also provided interesting results. Ti_3SiC_2 was successfully deposited for only the fourth time in over 25 years. Although the microstructures of deposited films were too complicated to permit extraction of kinetic data, the composition and morphology of these films were determined over a wide temperature range by extensive use of XRD, EDS, and SEM. Nearly pure Ti_3SiC_2 was deposited at 1300°C while Ti_3SiC_2-TiC composites were co-deposited at 1100 and 1200°C. At high temperature, a TiC boundary layer formed between the coating and the substrate, and periodically a thinner TiC layer was formed between regions of Ti_3SiC_2. Future thermodynamic calculations might include excess carbon as an input condition in order to determine to what extent, if any, a carbon substrate would influence the deposition diagrams. Such results would be pertinent to the early stage of deposition. Also, at least some of the Ti_3SiC_2 grains formed as a lamella structure with TiC. This would suggest that the nucleation and growth of Ti_3SiC_2 is somewhat dependent on TiC, which might be the kinetic hindrance unaccounted for by thermodynamic calculations. At all temperatures, Ti_3SiC_2 showed considerable preferred orientation, in which basal planes were deposited perpendicular to the substrate. Significant effort was focused on determining the temperature dependence of this orientation. Some Ti_3SiC_2 was deposited with basal planes parallel to the substrate at 1100-1200°C.

ACKNOWLEDGEMENTS

We appreciate the financial support and technical guidance provided by Dr. Alexander Pechenik of the Air Force Office of Scientific Research, Dr. Liselotte Schioler of the National Science Foundation, and First Lieutenant Kenneth A. Self of Wright Laboratories.

REFERENCES

1. S. Kumar, R. N. Singh, *Acta Metallurgical et Materialia*, "Effects of Fiber Coating Properties on the Crack Deflection and Penetration in Fiber-Reinforced Ceramic Composites" **1997**, 45[1], 4721-4731.
2. L. R. Hwang, J. W. Fergus, H. P. Chen, and B. Z. Jang, *Composites Science and Technology,* "Interface Compatibility in Ceramic-Matrix Composites" **1996**, 56, 1341-1348.
3. N. Chawla, J. W. Holmes, and R. A. Lowden, *Scripta Metallurgical et Materialia*, "The Role of Interfacial Coatings on the High Frequency Fatigue Behavior of Nicalon/C/SiC Composites" **1996,** 35[12], 1411-1416.
4. D. H. Kuo, W. M. Kriven, *Ceramic Engineering Science Proceedings*, "Microstructure and Mechanical Response of Lanthanum Phosphate/Yittrium Aluminate and Yittrium Phosphate/Yittrium Aluminate Systems" **1990**, 11[2], 70-74.
5. P. Morgan, D. Marshal, *Material Science and Engineering*, "Functional Interfaces for Oxide/Oxide Composites" **1993**, A162, 15-25.

6. K. K. Chawla, M. K. Ferber, Z. R. Xu, R. Venkatesh, *Materials Science and Engineering*, "Interface Engineering in Alumina/Glass Composites" **1993**, A162, 35-44.

7. C. Racault, F. Langlais, R. Naslain, *Journal of Material Science*, "Solid State Synthesis and Characterization of the Ternary Phase Ti_3SiC_2" **1994**, 29[13], 3384-3391.

8. M. W. Barsoum, T. El-Raghy, *Journal of the Electrochemical Society*, "Oxidation of Ti_3SiC_2 in Air" **1997**, 144[7], 2508-2516.

9. W. J. Lackey, S. Vaidyaraman, K. L. More, *Journal of the American Ceramic Society*, "Laminated C-SiC Matrix Composites Produced by CVI" **1997**, 80[1], 113-116.

10. J. Nickl, K. K. Schweitzer, P. Luxenberg, "Chemical Vapor Deposition of the System Ti-Si-C and Ti-Ge-C," Proc. 3rd Conf. on CVD, Salt Lake City, Utah **1972**.

11. T. Goto, T. Hirari, *Mat. Res. Bul.*, "Chemical Vapor Deposition of Ti_3SiC_2" **1987**, 22, 1195-1201.

12. C. Racault, F. Langlais, R. Naslain, Y. Kihn, *J. Mat. Sci.*, "On the Chemical Vapor Deposition of Ti_3SiC_2 from $TiCl_4$-$SiCl_4$-CH_4-H_2 Gas Mixture: Part II, An Experimental Approach" **1994**, 29[15], 3941-48.

13. G. Eriksson, *Acta Chemical Scandanavia*, "Thermodynamic Studies of High Temperature Equilibria, III. Solgas, a Computer Program for Calculating the Composition and Heat Conduction of an Equilibrium Mixture" **1971**, 25, 2651-2658.

14. G. Eriksson, *Chem. Scr.*, "Thermodynamic Studies of High Temperature Equilibria, III, Solgas, a Computer Program for Calculation of Equilibrium Compositions in Multiphase Systems" **1975,** 8, 100-103.

15. T. M. Besmann, "SOLGASMIX-PV, A Computer Program to Calculate Equilibrium Relationships in Complex Computer Systems," ORNL/TM-5775, Oak Ridge National Laboratory, Oak Ridge, Tennessee, April **1975**.

16. E. Pickering, "Chemical Vapor Deposition of Ti_3SiC_2," M.S. Thesis, Georgia Institute of Technology, Atlanta, Georgia, June (**1998**).

17. JANAF Thermochemical Tables, 3rd ed., Parts I and II; *J. Phys. Chem. Ref. Data* **1985**, 14, Supplement No. 1.

18. O. Kubaschewski, E. Evans, *Metallurgical Thermochemistry*, Vol. 1, Permagon Press, New York, New York **1958**.

19. J. Engqvist, C. Meyers, J. O. Carlsson, *Journal of the Electrochemical Society* **1992**, 139, 3197-3205, "Selective Deposition of $TiSi_2$ from H_2-$TiCl_4$ Gas Mixtures and Si: Aspects of Thermodynamics Including Critical Evaluation of Thermodynamic Data in the Ti-Si System."

20. C. Vahlas, P. Y. Chevalier, E. Blanquet, *Calphad* **1989,** 13, 3, 273-292, "A Thermodynamic Evaluation of Four Si-M (M = Mo, Ta, Ti, W) Binary Systems."

21. C. Racault, F. Langlais, C. Bernard, *Journal of Materials Science* **1994**, 29, 1, 5023-5040, "On the Chemical Vapor Deposition of Ti_3SiC_2 from $TiCl_4$-$SiCl_4$-CH_4-H_2 Gas Mixture: Part 1, A Thermodynamic Approach,".

22. Sanker Sambasivan, "Thermochemistry of Ceramic-Metal Reactions in Ti-Si-N and Ti-Si-C Systems at High Temperatures and Pressures," Ph.D. Thesis, Arizona State University, December **1990**.

23. B. D. Culity, *Elements of X-Ray Diffration*, 2nd ed., Addison-Wesley Publishing Company, **1978**.

24. M. W. Barsoum, T. El-Raghy, *Journal of the American Ceramic Society* **1996**, 79, 7, 1953-1956 "Synthesis and Characterization of a Remarkable Ceramic: Ti_3SiC_2."

LIST OF TABLES

Table I. Run Conditions for CVD of Ti_3SiC_2

Run Number	Target Flow Rates (cm^3/min)				α	Temperature (°C)	Pressure (kPa)	Time (min)
	$TiCl_4$	$SiCl_4$	CCl_4	H_2				
1,9,5	17.5	17.5	12.5	2000	42.1	1100,1200,1300	40.0	150
2,10,6	25.0	17.5	12.5	2000	36.4	1100,1200,1300	40.0	150
3,11,7	17.5	25.0	12.5	2000	36.4	1100,1200,1300	40.0	150
4,12,8	25.0	25.0	12.5	2000	32.0	1100,1200,1300	40.0	150

Table IV. Linear regression statistics for (hkl) ratios against temperature

(hkl)	A (slope) Constant	A (slope) Sig. level	B (intercept) Constant	B (intercept) Sig. level	R^2
(008)	-9.5454E-04	0.0276*	1.2770	0.0175	58.2%
(101)	2.1381E-03	0.0857	-0.1691	0.8960	41.3%
(104)	-4.0418E-03	0.0008	5.8209	0.0003	86.7%

*Indicates 97% confidence that temperature influences crystallographic orientation.

LIST OF FIGURES

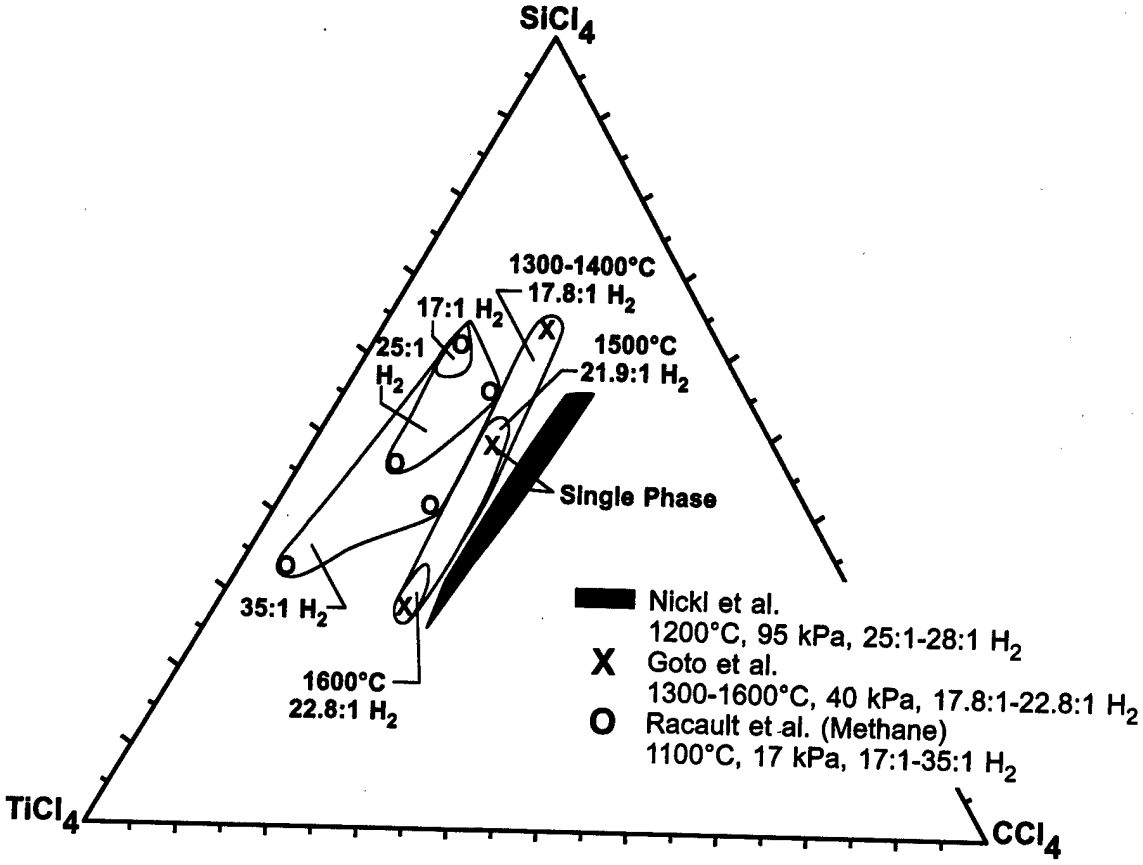

Figure 1. Review of the CVD of Ti_3SiC_2

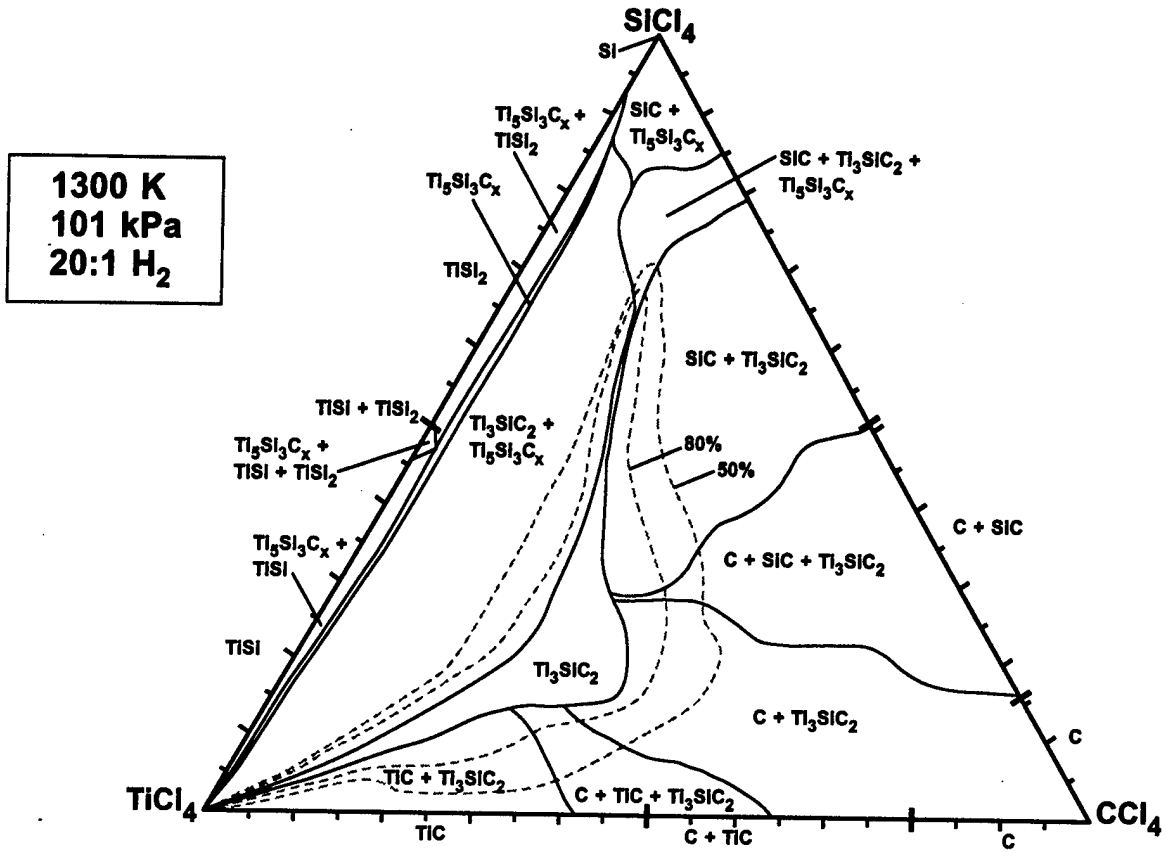

Figure 2. Calculated deposition diagram for the middle condition in the study.

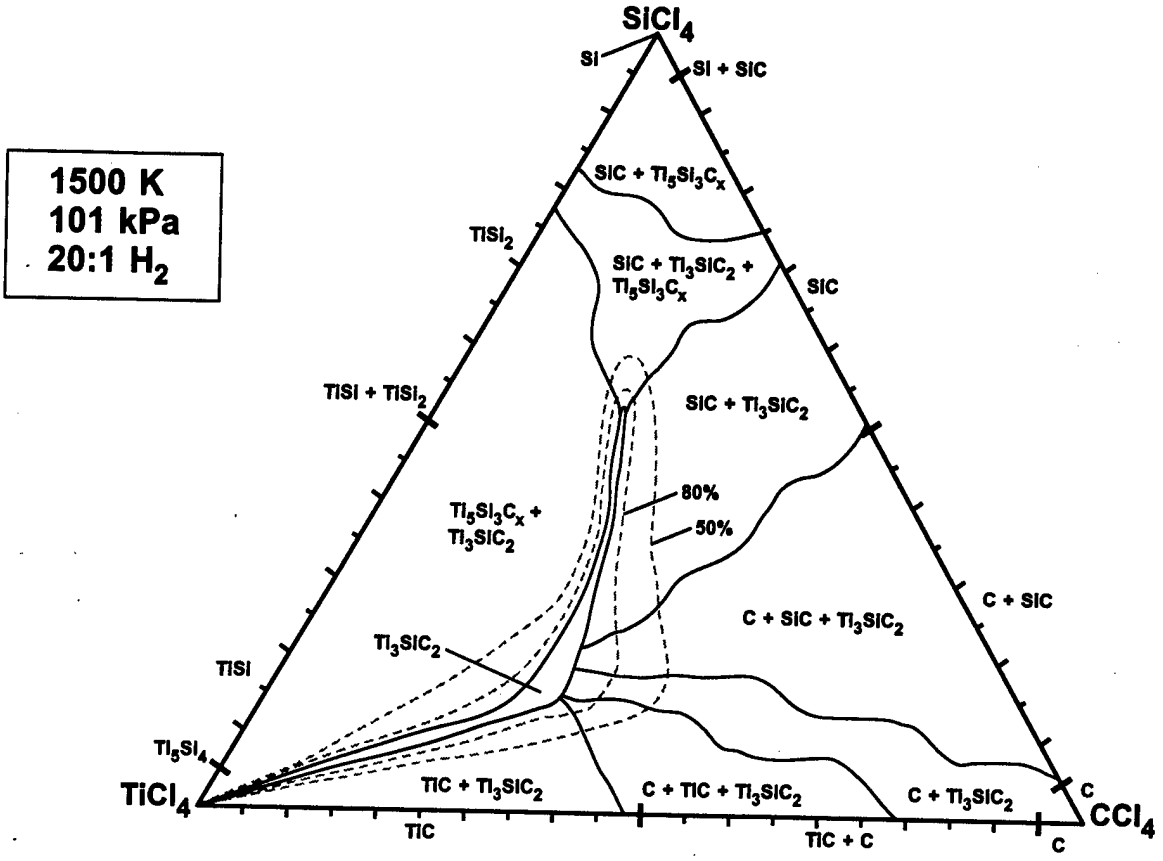

Figure 3. Calculated deposition diagram for the conditions 1500K, 101 kPa, α = 20:1. The dramatic change in the single phase field of Ti_3SiC_2 demonstrates the sensitivity of its thermodynamic data to deposition temperature.

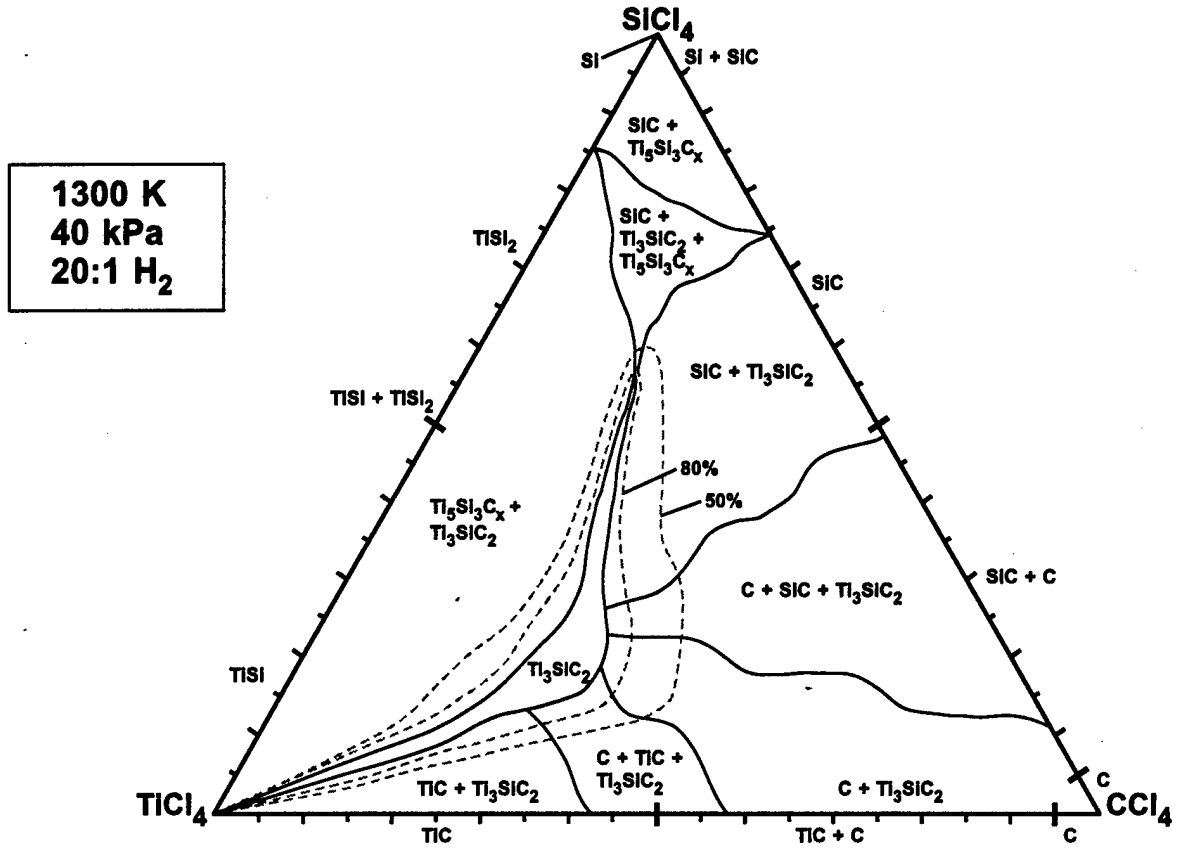

Figure 4. Calculated deposition diagram for the conditions 1300K, 40 kPa, and α = 20:1.

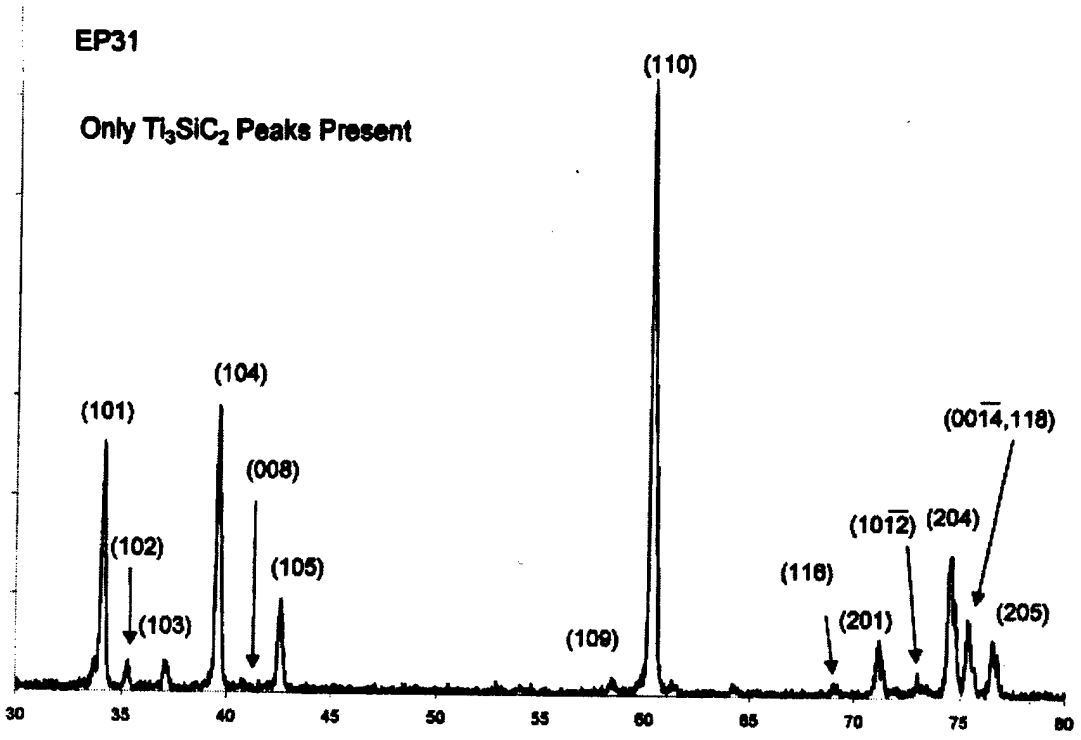

Figure 5. XRD pattern for EP31 deposited at 1300°C. Only Ti_3SiC_2 peaks are evident and peaks from basal planes show little intensity. This suggests highly textured Ti_3SiC_2.

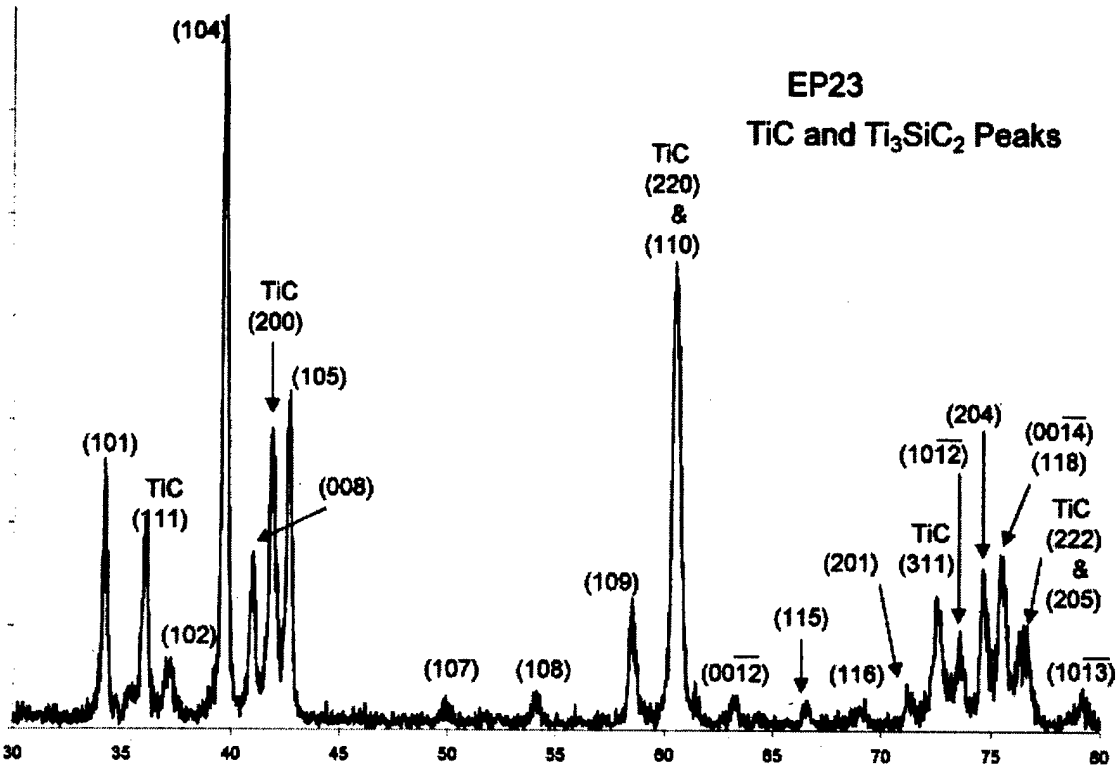

Figure 6 . XRD pattern for EP23 deposited at 1100°C. The pattern shows TiC and Ti_3SiC_2 peaks, with significant intensity from both phases.

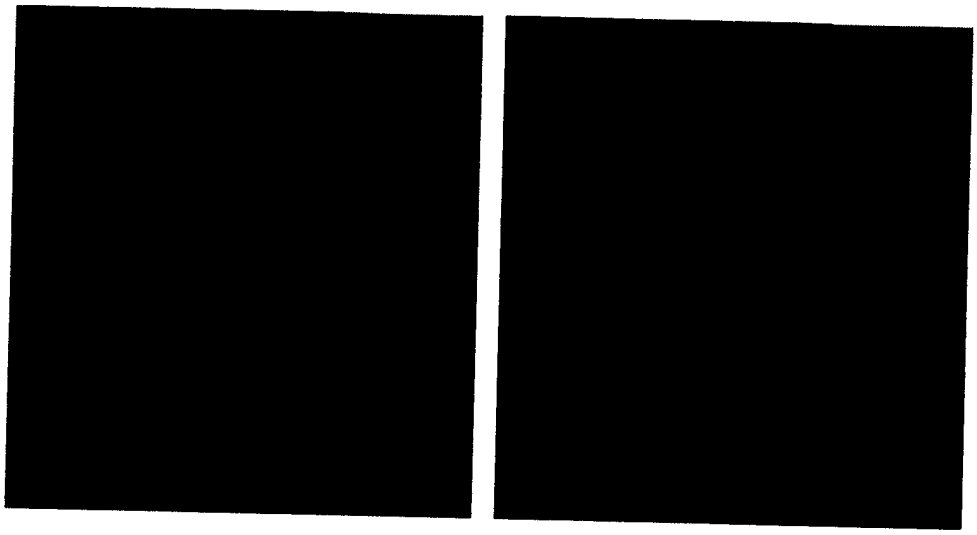

Figure 7. a) Surface morphology and b) cross section of coatings grown at 1300°C.

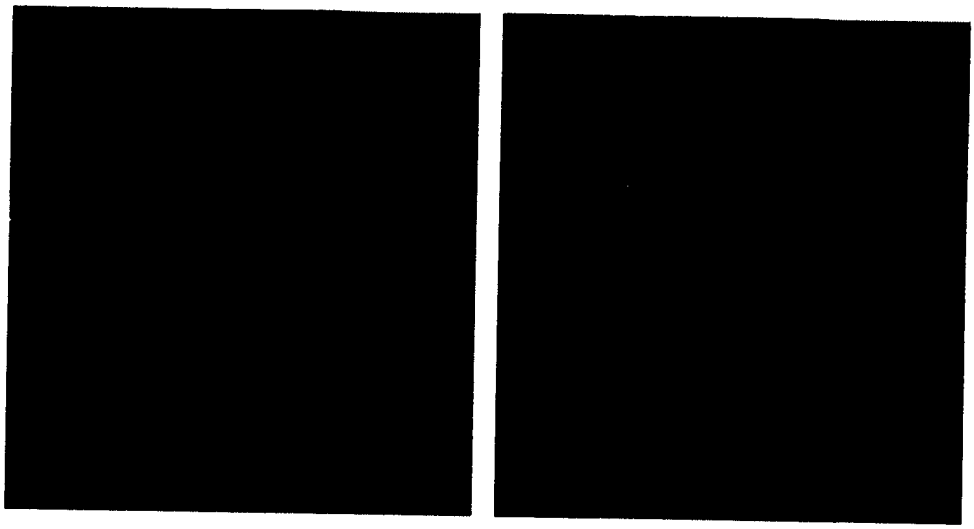

Figure 8. a) Surface morphology and b) cross section of coatings grown at 1100°C.

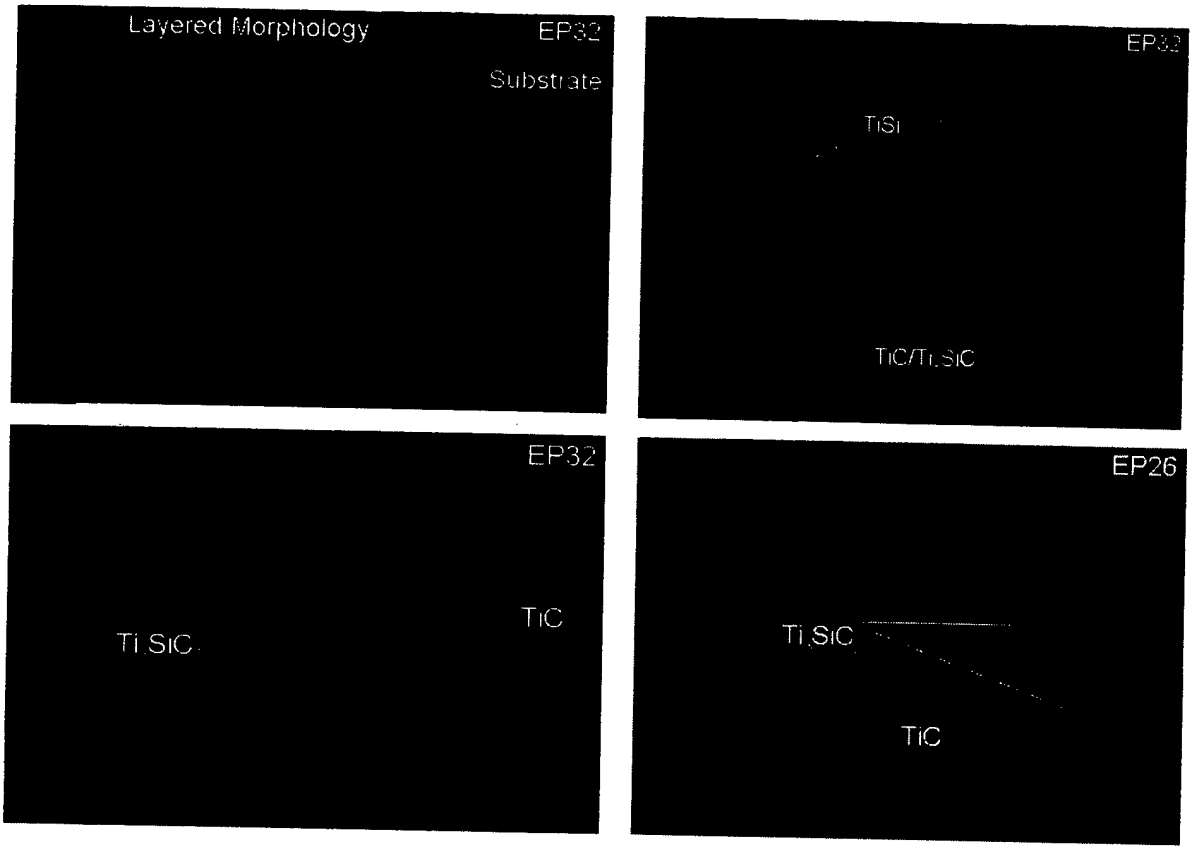

Figure 9. SEM micrographs of polished and etched cross sections of films grown at 1100°C showing a) layers of TiC, Ti_3SiC_2, and $TiSi_2$ formed by differing etch rates, b) continuous $TiSi_2$ layers and TiC/Ti_3SiC_2 co-deposition, c) high resolution of Ti_3SiC_2 grains in TiC matrix, and d) lower resolution Ti_3SiC_2 grains in TiC matrix.

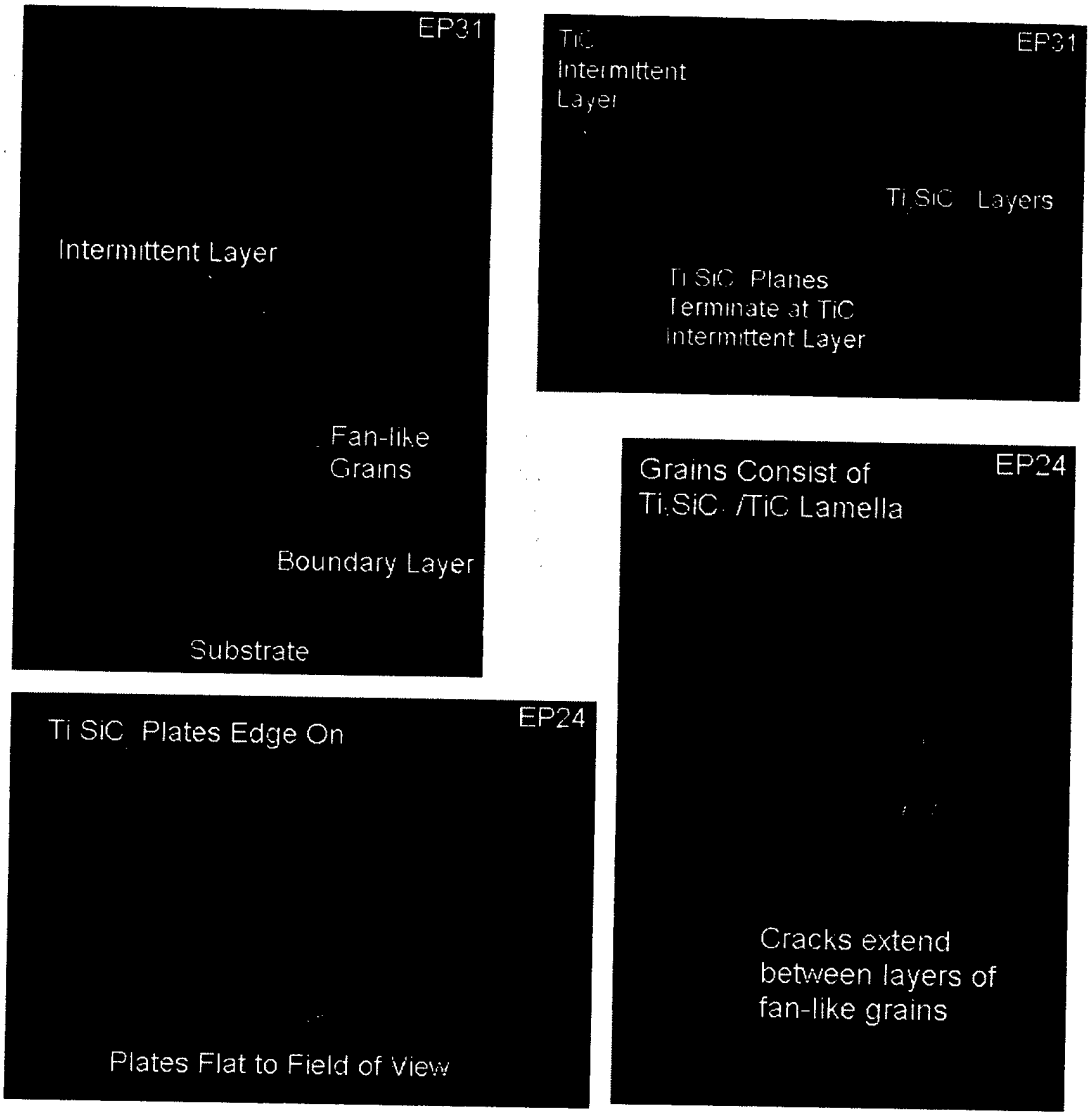

Figure 10. SEM micrographs of polished and etched cross sections of films grown at 1300°C showing a) TiC boundary and intermittent layers between fan-like grains of Ti_3SiC_2, b) interface between Ti_3SiC_2 and intermittent TiC layer, c) Ti_3SiC_2 grains seen with various orientation, and d) crack deflection in Ti_3SiC_2 and lamella structure of fan-like grains.